Mon. Not. R. Astron. Soc. **000**, 000–000 (0000)   Printed 29 June 2012   (MN LaTeX style file v2.2)

arXiv:1206.6634v1 [astro-ph.HE] 28 Jun 2012

Particle transport in microturbulence and acceleration performances of relativistic shocks

Illya Plotnikov,[1]⋆ Guy Pelletier,[1]† and Martin Lemoine,[2]‡
[1] *UJF-Grenoble 1 / CNRS-INSU, Institut de Planétologie et d'Astrophysique de Grenoble (IPAG) UMR 5274, Grenoble, F-38041, France.*
[2] *Institut d'Astrophysique de Paris, CNRS, UPMC, 98 bis boulevard Arago, F-75014 Paris, France*

Accepted —-. Received —-; in original form —-

ABSTRACT

Collisionless relativistic shocks have been the focus of intense theoretical and numerical investigations and these interesting physics have a direct impact on the generation of energetic particles and the interpretation of gamma ray spectra. The Fermi acceleration process that takes place in these shocks is intimately linked with the excitation of micro-turbulence responsible for the shock formation, electron heating and supra-thermal tail generation that in turn excites micro-turbulence, developing thus a self-sustaining phenomenon. In this paper we discuss the development of the micro-turbulence and we investigate two important issues: firstly the transport of supra-thermal particles in the excited microturbulence upstream of the shock and its consequences for the efficiency of the Fermi process; secondly, the preheating process of the incoming background electrons as they cross the shock precursor and experience relativistic oscillations in the electric field of the micro-turbulence. We emphasize the importance of the motion of the electromagnetic disturbances relatively to the background plasma and to the shock front. The investigation is carried out for the two major instabilities involved in the precursor of relativistic shocks, the filamentation instability and the oblique two stream instability. Bearing in mind these new results, we analyze the performance of the Fermi acceleration process in various high energy sources and especially in the termination shock of gamma-ray bursts. We emphasize the high efficiency of a collisionless ultra-relativistic shock for accelerating electrons and radiating a synchrotron-like photon spectrum up to several GeV.

Key words: relativistic shocks – micro-turbulence – transport of particles

1 INTRODUCTION

The micro-physics of collisionless relativistic shocks has been intensively investigated during these last years, both through numerical works and theoretical ones, especially since the remarkable work of Spitkovsky (2008a,b). The physics of those shocks describes the interplay between three phenomena, namely, the shock formation by reflecting back a fraction of the incoming particles, the generation of micro-turbulence by the reflected or back scattered particles that interact with the incoming plasma, and the development of the Fermi process. Much progress has been achieved within a few years through the development of theoretical and numerical works. Although the numerical simulations cannot reach the highest energies involved in the astrophysical phenomena, these works are already precise enough for inferring astrophysical consequences.

The physics of a relativistic shock is governed by few parameters, its Lorentz factor $\Gamma_{\rm s}$, the density of the ambient or upstream medium n and its magnetic field B_0. These two parameters determine two essential physical quantities, namely, the mass energy density ρc^2 which fixes the incoming energy to the shock front, $\Gamma_{\rm s}^2\rho c^2$, and the magnetization parameter σ that measures the ratio of magnetic energy flux crossing the shock over the incoming energy density:

$$\sigma \equiv \frac{B_{\rm t|f}^2}{4\pi\Gamma_{\rm s}^2\rho c^2} = \frac{B_0^2}{4\pi\rho c^2}\sin^2\theta_{\rm B}\ , \tag{1}$$

where $B_{\rm t|f} = \Gamma_s B_0 \sin\theta_B$ is the transverse component of the background magnetic field in the shock front rest frame, θ_B being the angle of the magnetic field with respect to shock normal, measured in the upstream rest-frame. Numerical simulations provide two essential parameters for astrophysical applications, namely the conversion factor $\xi_{\rm cr}$ of the incoming energy into cosmic rays, and the conversion factor $\xi_{\rm B}$ into magnetic energy:

$$P_{\rm cr} = \xi_{\rm cr}\Gamma_{\rm s}^2\rho c^2 \tag{2}$$

$$\frac{\overline{B}_{\rm |f}^2}{4\pi} = \xi_{\rm B}\Gamma_{\rm s}^2\rho c^2 \tag{3}$$

⋆ e-mail:`illya.plotnikov@obs.ujf-grenoble.fr`
† e-mail:`guy.pelletier@obs.ujf-grenoble.fr`
‡ e-mail:`lemoine@iap.fr`

where the cosmic ray pressure $P_{\rm cr}$ and the level of magnetic turbulence $\overline{B}_{|\rm f}$ are measured at the shock front. These two crucial parameters $\xi_{\rm cr}$ and$\xi_{\rm B}$ are expected to be on the order of $1-10$ percent (Sironi & Spitkovsky 2011a). Actually the cosmic rays are considered, as shown by numerical simulations and explained by theory, as the source of magnetic, and more generally electro-magnetic, turbulence. Indeed the collisionless shock forms by reflecting back a fraction of incoming particles on a barrier that can be due to the mean field, helped by an electrostatic potential when the plasma in composed of protons and electrons, or by the growth of electromagnetic waves, that in turn, triggers micro-instabilities. Particle acceleration has been observed in PIC simulations of unmagnetized relativistic shocks (Spitkovsky 2008b; Keshet et al. 2009; Martins et al. 2009; Sironi & Spitkovsky 2009, 2011a), and indeed one must expect the development of the Fermi process when the magnetization is very weak (Lemoine & Pelletier 2010), because microturbulence can then grow and provide the necessary scattering; this picture has been validated by the recent PIC simulations of Sironi & Spitkovsky (2011a). In this context of a proton electron plasma of low magnetization, the reference time scale is $\omega_{\rm pi}^{-1}$ and the spatial scale of reference is the inertial scale of protons $\delta_{\rm i} \equiv c/\omega_{\rm pi}$.

A collisionless relativistic shock at low magnetization is mostly governed by the development of two micro-instabilities that take place in the precursor, generated by the reflection of a part of incoming particles, namely the Weibel or filamentation instability (Medvedev & Loeb 1999) and the oblique two stream instability (hereafter OTSI; Fainberg et al. 1970, Bret et al. 2005). Because the upstream mean magnetic field in the front frame is generically almost perpendicular to the shock normal, it limits the penetration of reflected particles in the upstream flow; even weak it puts severe constraints to the growth of the instabilities by limiting the interaction length and the higher the Lorentz factor of the shock the weaker the value of the magnetization parameter below which the growth of the unstable modes is allowed (Lemoine & Pelletier 2010, 2011a). In the presence of a mean field, the efolding length scale ($\ell_{\rm g} \sim \xi_{\rm cr}^{-1/2}\delta_{\rm i}$) is shorter than the length of the foot, or the penetration length of reflected protons, $\ell_{\rm foot} = r_{\rm L,0}(1-\beta_{\rm s})/\Gamma_{\rm s} \sim \delta_{\rm i}/(2\Gamma_{\rm s}\sqrt{\sigma})$, when the magnetization is as small as $\sigma \lesssim \xi_{\rm cr}/4\Gamma_{\rm s}^2$. The most unstable mode with decreasing magnetization is the OTSI with the condition $\sigma < \xi_{\rm cr}^{2/3}/\mu^{1/3}\Gamma_{\rm s}^2$, where $\mu \equiv m_e/m_p$ (Lemoine & Pelletier 2010). Its role in the development of relativistic shocks is still unclear and this paper aims at shedding light on this issue. Then for weaker magnetization, precisely when $\sigma < \xi_{\rm cr}/\Gamma_{\rm s}^2$ (Lemoine & Pelletier 2010), Weibel modes can grow and the turbulent state so created allow particle scattering off small scale magnetic disturbances (filaments), and relativistic Fermi acceleration can develop. The scattering and diffusion of the particles in a small scale static and isotropic turbulence superposed on a mean field has been investigated numerically and theoretically in a previous paper (Plotnikov et al. 2011). In this paper we emphasize the issue of the motions of the magnetic disturbances and their anisotropy. With the studies of particle transport in both types of micro-turbulence, Weibel and OTSI, we draw their consequences for the collisionless relativistic shock formation, for electron pre-heating and for the performance of the Fermi process at astrophysical relativistic shocks.

For completeness, we mention that there are also relevant instabilities triggered by the compensation current in the background plasma that compensates the current carried by the reflected particles either along the mean field (but not generic) or across the mean field (unavoidable). For instance, reflected particles of opposite charge rotate in opposite direction in the transverse mean field and thus produce a very intense diamagnetic current responsible for a Buneman instability (Lemoine & Pelletier 2011a), and the instability is rapidly growing. Those current instabilities produce a turbulent heating of the electrons up to some temperature that reduces the anisotropy of the electron distribution function so that the instability saturates. Therefore these current instabilities participate in the process of preheating electrons, that arrive at the shock front with a relativistic temperature.

A collisionless relativistic shock can be described as a self-sustaining structure in which reflected particles generate a growing turbulence level that is responsible for particle reflection, for particle scattering and particle heating. Thus the key point is the identification of the relevant instabilities (one or two main) that produce modes able to accomplish this task. The main focus is on the Weibel instability that creates magnetic fluctuations on micro-scales, which stand in a frame that has to be specified and the OTSI that creates electromagnetic waves with an important electrostatic component in the background plasma. The waves excited in the background plasma cannot carry an energy density exceeding its mass energy density, so it can be written $U_{\rm w} = \xi_{\rm w}\rho c^2$ with $\xi_{\rm w} < 1$. In the frame moving with the shock front, the energy density is $\Gamma_{\rm s}^2\xi_{\rm w}\rho c^2$, the conversion factor into waves $\xi_{\rm w}$ being expected to be a sizable fraction in order to participate at both the shock formation and the generation of a supra-thermal tail. The pressure of relativistic particles can reach a comparable level, even a little larger since they are the cause of the instabilities. The first generation of reflected particles constitutes the main content of supra-thermal particles that pervade the ambient plasma with an energy density much larger than ρc^2 as measured in the frame of the ambient plasma. Its interaction with the background plasma can be described perturbatively as long as the proton beam of (apparent) density $n_{\rm b}$ and Lorentz factor $\gamma_{\rm b}$ is such that $\omega_{\rm pb} \ll \omega_{\rm p}$, which amounts to $n_{\rm b}/\gamma_{\rm b} \ll n/\mu$; now for a beam reflected by a shock, $n_{\rm b} = \xi_{\rm cr}\Gamma_{\rm s}^2 n$ and $\gamma_{\rm b} \sim \Gamma_{\rm s}^2$; thus the weak interaction criterium becomes $\xi_{\rm cr} \ll 1/\mu$, which is always realized.

The weak interaction of the very energetic beam with the ambient (or upstream) plasma renders the calculation of instability convenient in the frame of the background plasma, but, because of the tremendous energy of the beam, a saturation process through beam particle trapping or resonance broadening cannot be expected, as will be checked further on. The only nonlinear effects that can be relevant in the context of relativistic shock physics are nonlinear wave interactions, in particular the effects caused by the ponderomotive force associated with the instability wave.

The reflection of incoming protons, electron preheating and the motion of scattering centers are entangled issues and will be investigated step by step. The paper is organized as follows. In Section 2, we emphasize the important issue of the motion of the frame in which the Weibel filaments are static, an issue which has not been addressed yet, to our knowledge. We also summarize previous findings on a similar issue for the OTSI mode. We investigate the influence of the motion of the electromagnetic modes on the reflection process at the shock front. In Section 3 we study the transport of supra-thermal particles in both Weibel and OTSI turbulence, on the basis of numerical simulations of test particle propagation. Section 4 is devoted to the issue of electron pre-heating. We show that the relativistic oscillation of the incoming background electrons in the electric field of the micro-turbulence modes lead to efficient preheating on a short timescale. In Section 5 we apply our results to the concrete case of the external relativistic shock of a gamma-ray burst; we emphasize their capability to efficiently accelerate electrons so that it can radiate an extended synchrotron-like spectrum up to GeV photons. However we briefly show the difficulty to achieve ultra-high energies for protons in those shocks. In Section 6 we discuss possible sites of ultra-high energy cosmic rays (UHECR) generation. We summarize our results in Section 7.

2 MICRO-TURBULENCE IN THE PRECURSOR OF COLLISIONLESS WEAKLY MAGNETIZED RELATIVISTIC SHOCKS

2.1 The frame of magnetic filaments

Consider first the growth of magnetic perturbations due to Weibel instability triggered by a beam of velocity $\upsilon_{\rm b}$ and Lorentz factor $\gamma_{\rm b} = (1-\upsilon_{\rm b}^2/c^2)^{-1/2} \sim \Gamma_{\rm s}^2$ (upstream frame), interacting with a background plasma of density n at rest; at a shock wave, the beam of returning particles carries an energy density $\xi_{\rm cr}\gamma_{\rm b}^2 n m_p c^2$, so that the beam plasma frequency $\omega_{\rm pb} \sim \xi_{\rm cr}^{1/2}\mu^{1/2}\omega_{\rm pe}$, with $\omega_{\rm pe}$ the background electron plasma frequency (see Lemoine & Pelletier 2010 for details). In the upstream rest frame, the efolding length scale of the instability is written

$$\ell_{\rm g} \equiv c/\Im\omega \sim \xi_{\rm cr}^{-1/2}\delta_{\rm i} \ , \tag{4}$$

the detailed growth rate (see appendix A) being

$$\gamma_{\rm inst} \equiv \Im\omega = \sqrt{\xi_{\rm cr}}\omega_{\rm pi}\,\frac{\beta_{\rm b}k_\perp\delta_e}{(1+k_\perp^2\delta_e^2)^{1/2}} \ . \tag{5}$$

In the above expression and throughout this paper, $k_\perp$ represents the wavenumber component transverse to the shock normal, i.e. tangential to the shock front, while the (longitudinal) wavenumber component along the shock normal is written $k_\parallel$. For the filamentation mode, $k_\perp \gg k_\parallel$. In general, one takes the limit $k_\parallel \to 0$, which leads to the above aperiodic mode with $\Re\omega = 0$. However, for a small, but finite longitudinal wave number $k_\parallel$, the Weibel modes have a non-vanishing real frequency which indicates that these magnetic filaments propagate at high velocity. Considering first the case of a cold electron background:

$$\omega_r = k_\parallel \upsilon_{\rm b}\left(1-\xi_{\rm cr}\mu\frac{\gamma_{\rm b}^{-2}+k_\perp^2\delta_e^2}{1+k_\perp^2\delta_e^2}\right) \ . \tag{6}$$

We remark that this phase velocity is consistent with the result obtained in the center of mass frame of the counter streaming configuration when $\gamma_{\rm b} \simeq 1$; for $\mu = 1$ and $\xi_{\rm cr} = 1/2$, we find $\upsilon_\phi = \upsilon_{\rm b}/2$, which corresponds to a vanishing phase velocity in the center of mass frame. In the upstream rest frame, these waves are quasi-electromagnetic waves with the electric field $\mathbf{E}$ mostly oriented along the beam (shock normal), a dominant magnetic component perpendicular to both $\mathbf{k}_\perp$ and $\mathbf{E}$, and finally a small electrostatic component of $\mathbf{E}$ along $\mathbf{k}_\perp$. The magnetic component remains the most intense component despite a phase velocity close to c along the normal direction because $B \simeq (k_\perp/k_\parallel)E$, and the energy density is mostly magnetic. The fact that they have a phase velocity close to c implies that they suffer negligible Landau damping (as long as the thermal velocity of the electrons is small).

If the background electrons have been preheated to relativistic temperatures, their electromagnetic response and therefore the instability are modified. The maximum growth rate remains unchanged, $\Im\omega \sim \xi_{\rm cr}^{1/2}\omega_{\rm pi}$, but the spatial scale at which maximum growth occurs is now larger because the electron inertial scale is enlarged by a factor $\sqrt{\bar\gamma_e}$, with $\bar\gamma_e$ the mean electron thermal Lorentz factor in the upstream rest frame $\bar\gamma_e = 1 + 3T_e/m_e c^2$. This latter spatial scale tends to $\delta_{\rm i}$ in the limit of equipartition, meaning $\bar\gamma_e \to m_p/m_e$. In a relativistically hot background, the phase velocity of the modes along the beam direction is considerably slowed down, but remains nonetheless relativistic for reasonable values. If one defines $\gamma_{\rm m}$ as the Lorentz factor associated to the mode velocity along the beam direction, the calculations presented in Appendix A indicate

$$\gamma_{\rm m} \simeq \left[(\bar\gamma_e\mu\xi_{\rm cr})^{1/2} + 2\xi_{\rm cr}\right]^{-1/2} \ . \tag{7}$$

Equipartition corresponds to $\bar\gamma_e\mu = 1$, and prior to equipartition $\bar\gamma_e\mu < 1$. For relativistically hot electrons far from equipartion, $\gamma_{\rm m} \simeq (2\xi_{\rm cr})^{-1/2}$, then $\gamma_{\rm m} \sim (\xi_{\rm cr}\mu\bar\gamma_e)^{-1/4}$ when $\bar\gamma_e\mu > \xi_{\rm cr}$, and finally the lowest value of $\gamma_{\rm m} \sim 2$ is reached at equipartion. This value is much smaller than that obtained in the cold electron background, $\gamma_{\rm m} \sim (\xi_{\rm cr}\mu)^{-1/2}$, but it nevertheless plays an important role in what follows.

Note that the filamentation instability in the usptream of a relativistic shock is quenched when $\Gamma_{\rm s} < (\xi_{\rm cr}\mu)^{-1/2}$ as long as the electrons are kept cold due to the finite angular dispersion of the beam (Rabinak et al. 2011, Lemoine & Pelletier 2011a). In a hot background however, the filamentation instability remains strong, even when the beam angular dispersion is taken into account.

So clearly, the Weibel filaments that can be considered as wave packets of transverse size $\ell_\perp \sim \bar\gamma_e^{1/2}\delta_e$ and extension in the normal direction $\ell_\parallel > \bar\gamma_e^{1/2}\delta_e$, but necessarily finite (at least because of the finite growth length in a precursor of finite extent), are unavoidably moving at high speed with respect to the ambient medium. This is a very important point that has not been taken into account in the literature, to our knowledge. They move at a highly relativistic velocity when the electrons are cold, with a Lorentz factor $\gamma_{\rm m} \simeq (\xi_{\rm cr}\mu)^{-1/2}$, which can be of several hundreds (typically for $\xi_{\rm cr} = 0.1$, $\gamma_{\rm m} \simeq 140$). When the electrons are relativistically hot, $\gamma_{\rm m}$ is more moderate. Three cases deserve attention: $\gamma_{\rm m} \sim \Gamma_{\rm s}$ where the filaments move more or less at the same speed as the shock front, $\gamma_{\rm m} < \Gamma_{\rm s}$ where the shock front catches up the filaments and the case where the filaments can even run faster than the shock for $\Gamma_{\rm s} < \gamma_{\rm m}$. In this latter case the generation of filaments might lead to shock reformation.

The filaments are static in the frame moving at $\beta_{\rm m}$ with respect to the background plasma, however in this frame they are no longer purely magnetic and comprise an electrostatic field of almost the same intensity as the magnetic field: $E'_\perp \simeq \gamma_{\rm m}B \simeq B'$, since $B' = \gamma_{\rm m}B$, with the prime denoting the quantity in the filament rest frame. The electromagnetic energy density in this frame is thus $U'_{\rm e.m.} = \gamma_{\rm m}^2 B^2/(4\pi)$. The electromagnetic flux that crosses the shock front, measured in the co-moving front frame is $S_{\rm e.m.|f} = V_{\rm s}\Gamma_{\rm s}^2 B^2/4\pi$.

The relative velocity of the filaments with respect of the shock front can be written

$$\beta_{\rm m|f} \simeq \frac{\gamma_{\rm m}^2-\Gamma_{\rm s}^2}{\gamma_{\rm m}^2+\Gamma_{\rm s}^2} \ , \tag{8}$$

and the associated Lorentz factor

$$\Gamma_{\rm m|f} = \frac{1}{2}\left(\frac{\gamma_{\rm m}}{\Gamma_{\rm s}} + \frac{\Gamma_{\rm s}}{\gamma_{\rm m}}\right) \ . \tag{9}$$

Let us look at their growth rate as measured in the shock front frame. As shown in the appendix B, the product $\gamma_{\rm g}\gamma_{\rm inst}$ is invariant under Lorentz transformations, where $\gamma_{\rm g}$ is the Lorentz factor associated with the group velocity. Thus the transformed growth rate is

$$\gamma_{\rm inst|f} = \sqrt{2}\omega_{\rm pe}\frac{\Gamma_{\rm s}\gamma_{\rm m}}{\Gamma_{\rm s}^2+\gamma_{\rm m}^2}\ , \tag{10}$$

which is maximum for $\gamma_{\rm m} = \Gamma_{\rm s}$, when the magnetic disturbances are standing in front frame.

The motion of the wave packets carries special importance when determining the condition for particle reflection, the level of electron pre-heating and also for the analysis of the Fermi process, as discussed in the following.

In the case of an ultra-relativistic shock in an electron positron plasma, $\gamma_{\rm m}$ is at most a few and the shock front catches up the magnetic disturbances ($\Gamma_{\rm s} \gg \gamma_{\rm m}$). The behavior is the same in a proton-electron plasma when $1 \ll \overline{\gamma}_e \lesssim m_p/m_e$.

The discussion about the motion of magnetic disturbances is also important for their transmission in the downstream flow. Indeed the relative motion of the upstream flow with respect to the downstream one is characterized by a relative Lorentz factor $\Gamma_{\rm r} = \Gamma_{\rm s}/\sqrt{2}$. Because the modes propagates at a speed $\upsilon_{\rm m}$ with respect of the upstream plasma, the Lorentz transform of their frequency and normal wave number to the downstream frame leads to

$$\begin{aligned} \omega' &= \Gamma_{\rm r}(\beta_{\rm m}-\beta_{\rm r})k_z c \simeq \frac{1}{2}\Gamma_{\rm r}k_z c\left(\frac{1}{\Gamma_{\rm r}^2}-\frac{1}{\gamma_{\rm m}^2}\right) \\ k'_z &= \Gamma_{\rm r}(1-\beta_{\rm r}\beta_{\rm m})k_z \simeq \frac{1}{2}\Gamma_{\rm r}k_z\left(\frac{1}{\Gamma_{\rm r}^2}+\frac{1}{\gamma_{\rm m}^2}\right) \end{aligned} \tag{11}$$

Thus, when $\gamma_{\rm m} \ll \Gamma_{\rm s}$, the modes are perceived as electromagnetic waves of the vacuum in the downstream frame, propagating backwards ($\omega' \simeq -k'_z c$). In the opposite extreme, they are perceived as forward propagating vacuum waves. The interesting case is when $\gamma_{\rm m} \sim \Gamma_{\rm s}$, where they are perceived as low frequency magnetic perturbations. However, one should stress here that the motion of the filament is calculated at the linear level, while the transmission of modes downstream proceeds in the highly nonlinear regime. Therefore it is not clear at present whether the above Eq. 11 applies to the transition; it should be taken with caution.

2.2 The role of OTSI turbulence

A priori the Weibel instability can produce all the effects expected to occur at a relativistic shock including Fermi acceleration. However the OTSI is unavoidable, and it even grows a little faster than the Weibel instability. The OTSI is a resonant instability of electron plasma waves ($\omega \simeq \omega_{\rm pe}$) with a sharp selection of the wave-vector component along the beam: $k_z = \omega_{\rm pe}/c$, and that grows much faster than the usual two stream instability (which has no transverse component of its wave-vector) when the transverse component of the wave-vector is of order $\omega_{\rm pe}/c$ also (see Fainberg et al. 1970, Bret et al. 2005). These modes are mostly electrostatic in the background plasma frame and partly electromagnetic and grow a little faster than Weibel mode in the precursor of a relativistic shock (Lemoine & Pelletier 2010), their frequency is slightly shifted by the beam with $\omega = \omega_{\rm pe}(1-|\delta|/2)$ and their growth rate $\Im\omega = \sqrt{3}\,2^{-4/3}|\delta|\omega_{\rm pe}$ with $|\delta| = \xi_{\rm cr}^{1/3}\mu^{1/3}$, whereas the growth rate of the Weibel modes scales as $\xi_{\rm cr}^{1/2}\mu^{1/2}\omega_{\rm pe}$ in the same cold background limit. The ratio of the electromagnetic component over the electrostatic one is of order $|\delta|$.

As discussed in Lemoine & Pelletier (2011a), Shaisultanov et al. (2011), the two stream instability becomes inhibited once the electrons are heated to ultra-relativistic temperatures and the Weibel instability becomes the dominant mode.

In order to study the dynamics of particles in the modes, it is interesting to move to the wave-frame where the particles experience a static electric field and a static magnetic field. The wave frame velocity with respect to the background plasma is $\beta_{\rm m} = 1-|\delta|/2$ and the corresponding Lorentz factor

$$\gamma_{\rm m} = |\delta|^{-1/2} \simeq \xi_{\rm cr}^{-1/6}\mu^{-1/6} \sim 5 \tag{12}$$

with respect of the background plasma. These mildly relativistic wave-packets are thus rapidly overtaken by the shock front.

As in the case of Weibel modes, the dynamics in OTSI modes is also governed by a couple of transverse fields of similar amplitude when one shifts to the rest frame in which these modes are static. A crucial difference however is that the OTSI mode appears as a high frequency quasi vacuum wave in the front frame, with a unique wavenumber along the normal direction, revealing a clear periodic pattern in that direction.

2.3 The reflection of incoming particles

The deviation of the incoming protons becomes significant when the level of magnetic fluctuations is such that the effective Larmor radius $\overline{r}_{\rm L} \sim \ell_{\|}$, where $\ell_{\|}$ denotes the coherence length of the magnetic disturbance in the normal direction. In order to properly state that condition, we must express it in the co-moving frame of the magnetic disturbances; indeed if one moves to another frame according the Lorentz transformation, the disturbances become time dependent and fully electromagnetic. Therefore we state that reflection is achieved when, in the proper frame of magnetic disturbances, $\overline{r}_{\rm L|m} \sim \ell_{\|,m}$; that estimate amounts to $e\overline{B}_{\rm |m}\ell_{\|,m} \sim \gamma_{\rm m}m_pc^2$ with $\ell_{\|,m} = \gamma_{\rm m}\ell_{\|}$ and $\overline{B}_{\rm |m} = \gamma_{\rm m}\overline{B}$. Since the electric field is of similar amplitude in the filament frame, the corresponding condition with the electric field component is that the energy of the incoming protons is comparable with the work done by the electric force over the scale $\ell_{\|}$. Therefore

$$\frac{\overline{B}_{\rm |m}^2}{4\pi} \sim \frac{\delta_{\rm i}^2}{\ell_{\|}^2}\rho c^2\ , \tag{13}$$

which leads to a magnetic conversion factor, as defined in the introduction,

$$\xi_{\rm B} \sim \frac{1}{\gamma_{\rm m}^2}\frac{\delta_{\rm i}^2}{\ell_{\|}^2} \sim (\xi_{\rm cr}\overline{\gamma}_e\mu)^{1/2}\frac{\delta_{\rm i}^2}{\ell_{\|}^2}\ \text{or}\ \xi_{\rm cr}\frac{\delta_{\rm i}^2}{\ell_{\|}^2}\ ; \tag{14}$$

the second estimate stems from the fact that the reflection occurs in the phase where the electrons are relativistically hot and thus $\gamma_{\rm m} \sim (\xi_{\rm cr}\overline{\gamma}_e\mu)^{-1/4}$ and the last one when $\overline{\gamma}_e\mu \leqslant \xi_{\rm cr}$. Furthermore we expect that the wave extension $\ell_{\|}$ (defined in the usptream frame) is not larger than the growth scale $\ell_{\rm g} = \xi_{\rm cr}^{-1/2}\delta_{\rm i}$, so that mode envelopes on scale $\ell_{\|}$ of a few $\delta_{\rm i}$ can produce the necessary reflection.

Under that condition a significant amount of incoming protons are reflected back and self-sustain that magnetic turbulence through the Weibel instability. When those conditions are fulfilled, the self-sustaining turbulence through the reflection of a fraction of incoming protons stabilizes at a level that remains much smaller than all other processes of nonlinear saturation such as proton trapping, resonance broadening. Indeed, the trapping of reflected beam protons requires that the level of micro-turbulence is such that the time scale of non-linear oscillation $\tau_{\rm nl} \equiv \ell_{\rm c}(\epsilon/\epsilon_\star)^{1/2}/c$ (where $\epsilon_\star = e\overline{E}'\ell_{\rm c}$) reaches the growth time $\omega_{\rm pb}^{-1}$; since $\omega_{\rm pb} = \xi_{\rm cr}^{1/2}\omega_{\rm pi}$, this amounts to $\epsilon_\star \sim \xi_{\rm cr}\epsilon\ell_{\rm c}^2/\delta_{\rm i}^2$, which is totally impossible with beam protons of energy $\epsilon \sim \Gamma_{\rm s}^2m_pc^2$. A similar conclusion can be drawn when one considers the resonance broadening effect, which stems from the fact that particle scattering or diffusion broadens the resonance of modes with the beam responsible for the instability. Indeed $\nu_\mathrm{s} > \omega_\mathrm{pb}$ would require $\epsilon_\star > \xi_\mathrm{cr}^{1/4}(\ell_\mathrm{c}/\delta_\mathrm{i})^{1/2}\epsilon$, which is impossible with a so high energy of beam protons.

2.4 Heating and transport in the micro-turbulence

In the Section that follows, we discuss in some details the scattering of supra-thermal particles and the heating process of background particles in the motional micro-turbulence upstream of the shock. These actually represent two different facets of a similar problem, namely particle transport in a time varying micro-turbulence. However, in the test particle picture that we adopt in the following, these two populations, the supra-thermal particles and the background electrons, differ one from the other by their wiggler parameter

$$a \;\equiv\; \frac{e\bar{E}'\ell'_\perp}{m_e c^2}\ , \tag{15}$$

as expressed in terms of the micro-turbulent electric field $\bar{E}'$ and transverse scale $\ell'_\perp$ in the wave frame. As discussed in the following, in the wave frame $\bar{E}'$ and $\bar{B}'$ are of the same order, so that there is no ambiguity in the definition of a.

Cold background electrons have a Lorentz factor $\gamma' \sim \gamma_\mathrm{m}$ in the wave frame, so that

$$\frac{a}{\gamma'} \;\simeq\; \xi_\mathrm{B}^{1/2}\frac{m_p}{m_e}\frac{\ell_\perp}{\delta_\mathrm{i}} \;\gg\; 1\ , \tag{16}$$

meaning that these electrons experience relativistic oscillations on a coherence length scale in the wave frame. Of course, as the electrons near equipartition, the ratio a/γ' becomes closer to unity.

Consider now a supra-thermal electron, with Lorentz factor γ in the upstream rest frame, becoming $\gamma' \simeq \gamma/\gamma_\mathrm{m}$ in the mode rest frame (assuming $\gamma \gg \gamma_\mathrm{m}$). The minimal Lorentz factor of supra-thermal electrons is $\gamma_\mathrm{min} \sim \Gamma_\mathrm{s}^2 m_p/m_e$ in the upstream frame, hence one can write

$$\frac{a}{\gamma'} \;\simeq\; \xi_\mathrm{B}^{1/2}\frac{\gamma_\mathrm{m}^2}{\Gamma_\mathrm{s}^2}\frac{\gamma_\mathrm{min}}{\gamma}\frac{\ell_\perp}{\delta_\mathrm{i}}\ , \tag{17}$$

which is expected to be much smaller than unity: recall that $\ell_\perp$ is expected of the order of δ_e if the background electrons are cold (in which case γ_m can be large if the Weibel instability is not quenched by the angular dispersion of the beam), but of order δ_i if the background electrons reach equipartition with the ions, in which case γ_m becomes of order of a few for the Weibel modes. Thus $a/\gamma' \ll 1$ for supra-thermal electrons, while $a/\gamma' \gg 1$ for the background electrons, typically.

Before discussing the transport of these particles in the upstream micro-turbulence, it may be useful to briefly recall how transport is thought to take place downstream of the shock. According to the numerical simulations of Chang et al. (2008), the micro-turbulence downstream of the shock appears mostly static and magnetic in the downstream rest frame. In Plotnikov et al. (2011), we have discussed in some detail the transport coefficients of high energy particles in such a micro-turbulence, accounting for the presence of a transverse background magnetic field.

One first defines the scattering frequency

$$\nu_\mathrm{s} = \frac{2}{3}\frac{c}{\ell_\mathrm{c}}\left(\frac{e\bar{B}\ell_\mathrm{c}}{\epsilon}\right)^2\ , \tag{18}$$

with ℓ_c the coherence scale of the fluctuations, $\bar{B} = \sqrt{B_0^2 + \delta B^2}$ the rms magnetic field and ϵ the particle energy, in the downstream frame. When there is no mean field, the spatial diffusion is isotropic and is simply described by the following diffusion coefficient

$$D = \frac{1}{3}\frac{\upsilon^2}{\nu_\mathrm{s}} \sim c\ell_\mathrm{c}\left(\frac{\epsilon}{e\bar{B}\ell_\mathrm{c}}\right)^2\ . \tag{19}$$

When there is a mean field, even weak, the spatial diffusion is anisotropic, because the scattering frequency becomes smaller than the Larmor frequency in the mean field at high energy, meaning that $\epsilon \gg e\bar{B}\ell_\mathrm{c}$. The diffusion along the mean field, $D_\parallel$ remains similar to the previous one, but the transverse diffusion $D_\perp$ is given by

$$D_\perp = \frac{\upsilon^2}{3}\frac{\nu_\mathrm{s}}{\omega_\mathrm{L,0}^2 + \nu_\mathrm{s}^2}\ , \tag{20}$$

with $\omega_\mathrm{L,0} \equiv eB_0\ell_\mathrm{c}/\epsilon$, similarly to classical diffusion. Thus instead of increasing like ϵ^2 at high energies, it reaches a maximum finite value $2c\ell_\mathrm{c}\bar{B}^2/(9B_0^2)$.

If one forgets this effect of the mean field, Fermi acceleration at shocks looses rapidly its efficiency because the acceleration time increases like ϵ^2. One might think that the mean field increase the acceleration efficiency by maintaining particles in the shock vicinity during a longer time, as in perpendicular non relativistic shock acceleration. This is not so however, because the large advection speed of the downstream relative to the shock easily beats the transverse diffusion of particles, which can set in only after a time ν_s^{-1}.

3 TRANSPORT OF SUPRA-THERMAL PARTICLES IN THE WAVE FRAME

In this Section, all the quantities are measured in the frame of magnetic disturbances, unless otherwise stated. In this frame the total energy of any particle is a constant of motion due to time translation invariance.

In the upstream frame, the wave-numbers of Weibel modes obey $k_\perp/k_\parallel \gg 1$ and $\Re\omega \ll k_\perp$, so that in the wave frame $k'_\perp/k'_\parallel \gg 1$ as well. Regarding OTSI modes, one finds $k_\perp \sim k_\parallel$ in the upstream frame, but Lorentz boosting to the wave frame gives predominance to the transverse wave-numbers. If, in a first approximation, the spatial dependence along the shock normal is disregarded, the normal component of the generalized momentum also becomes a constant of motion: $p_\parallel + eA_z(x,y) = C^{st}$. Thus the momentum of the particle is confined in a subset of the energy surface determined by $\Delta p_\parallel = e\Delta A_z$, where ΔA_z is the rms variation of the normal vector potential. In short, the assumption of translational invariance along the Weibel filaments leads to an inhibition of momentum diffusion, see also Jones et al. (1998) for similar issues. This is a crucial point which directly impacts the efficiency of acceleration, which requires transverse scattering in the absence of a mean field. As we discuss further below, the transverse momentum is subject to large angular variations in the transverse plane, which leads to spatial diffusion. In order to obtain pitch angle diffusion, it is thus necessary to consider the full 3D dependence of the magnetic fluctuations; this scattering will lead to spatial diffusion along the three directions.

Weibel modes propagate with a sub-luminal velocity $\boldsymbol{\upsilon}_\mathrm{m}$ along the beam ($\Re\omega = k_\parallel\upsilon_\mathrm{m}$) and thus have a rest-frame in which particles experience a static electric field and a static magnetic field. Similarly OTSI modes have a single sub-luminal phase velocity because the wave number along the beam is selected by a narrow resonance. For both cases the analysis of particle dynamics is suitable in the wave-frame, because this is the frame where the transport coefficients can be properly defined, where the distribution function tends to become more or less isotropized, and fundamentally, this is the proper frame of scattering centers involved in the Fermi process.

The Lorentz force acting in the wave-frame depends on the fields obtained by the Lorentz transform from the upstream plasma frame to the wave-frame:

$$
\begin{aligned}
\boldsymbol{E}'_{\parallel} &= \boldsymbol{E}_{\parallel}\\
\boldsymbol{E}'_{\perp} &= \gamma_{\rm m}(\boldsymbol{E}_{\perp} + \boldsymbol{\beta}_{\rm m}\times\boldsymbol{B}_{\perp})\\
\boldsymbol{B}'_{\parallel} &= \boldsymbol{B}_{\parallel}\\
\boldsymbol{B}'_{\perp} &= \gamma_{\rm m}(\boldsymbol{B}_{\perp} - \boldsymbol{\beta}_{\rm m}\times\boldsymbol{E}_{\perp})
\end{aligned}
$$

In the case of Weibel modes, $|E| \ll |B|$, and for $\gamma_{\rm m}$ large enough, at first approximation, $\boldsymbol{B}'_{\perp} \simeq \gamma_{\rm m}\boldsymbol{B}_{\perp}$ and $\boldsymbol{E}'_{\perp} \simeq \gamma_{\rm m}\boldsymbol{\beta}_{\rm m}\times\boldsymbol{B}_{\perp} \simeq \boldsymbol{\beta}_{\rm m}\times\boldsymbol{B}'_{\perp}$.

In the case of OTSI modes, in the upstream frame the modes are almost electrostatic $|\boldsymbol{B}| \ll |E|$, and $E_{\perp} \sim E_{\parallel}$ (oblique modes). Thus we neglected the contribution of $B_{\parallel}$ and $B_{\perp}$. The system is quite similar to the system derived for Weibel modes in their proper frame, since $\boldsymbol{E}'_{\perp} \simeq \gamma_{\rm m}\boldsymbol{E}_{\perp}$ and $\boldsymbol{B}'_{\perp} \simeq -\gamma_{\rm m}\boldsymbol{\beta}_{\rm m}\times\boldsymbol{E}_{\perp}$, which leads to $\boldsymbol{B}'_{\perp} \simeq -\boldsymbol{\beta}_{\rm m}\times\boldsymbol{E}'_{\perp}$. We will analyze the particle dynamics first in a 2D approximation, meaning $E'_{\parallel} \to 0$, $B'_{\parallel} \to 0$, and then in the complete 3D configuration ($E'_{\parallel} = E'_{\perp}/\gamma_{\rm m}$).

When going to the wave frame, the perpendicular coherence length remains unchanged, $\ell'_{\perp} = \ell_{\perp}$, while $\ell'_{\parallel} = \gamma_{\rm m}\ell_{\parallel}$. This section considers quantities in the wave frame, as made explicit by the primes.

3.1 Transport in 2D approximation

The particle dynamics can be further simplified, when one neglects the longitudinal components (z direction) $E'_{\parallel}$ et $B'_{\parallel}$ in a first approximation. Then the system reduces to:

$$
\begin{aligned}
\frac{{\rm d}p_x}{{\rm d}t} &= qE'_x(1+\beta_{\rm m}\beta_z) &(21)\\
\frac{{\rm d}p_y}{{\rm d}t} &= qE'_y(1+\beta_{\rm m}\beta_z) &(22)\\
\frac{{\rm d}p_z}{{\rm d}t} &= -q\beta_{\rm m}(\beta_x E'_x + \beta_y E'_y) &(23)
\end{aligned}
$$

where the relation $\boldsymbol{B}'_{\perp} = -\boldsymbol{\beta}_{\rm m}\times\boldsymbol{E}'_{\perp}$ has been inserted. Because $k'_z = \gamma_{\rm m}(k_z - \beta_{\rm m}\omega/c) \simeq k_z/2\gamma_{\rm m}$, for large $\gamma_{\rm m}$ the z dependence of the field can be neglected in a first approximation. The system is the same for both Weibel and OTSI modes.

Because the turbulent fields depend on two spatial variables (x, y), there are two invariants: the total particle energy, given by the Hamilton function

$$H = \epsilon(p) + q\Phi(x, y) \qquad (24)$$

and the generalized momentum

$$\pi_z = p_{\parallel} + qA_z(x, y)/c\,. \qquad (25)$$

These two potentials are related to one another: $A_z(x, y) = \Phi(x, y)$. Since the potential has a zero average and a finite rms value $\Delta\Phi$, the particle proper energy ϵ and its z-momentum $p_{\parallel}$ have well defined rms variations under the ergodic assumption: $\Delta\epsilon = \Delta p_{\parallel}c = e\Delta\phi$. These relations determine confinement regions in phase space and forbid some diffusion processes. The norm of the transverse momentum also has bounded variations. Indeed, considering the variation from initial values, $\delta\epsilon = \epsilon - \epsilon_0$, $\delta p_{\parallel} = p_{\parallel} - p_{\parallel,0}$, $\delta\boldsymbol{p}_{\perp} = \boldsymbol{p}_{\perp} - \boldsymbol{p}_{\perp,0}$, one exactly finds

$$2(\epsilon_0 - p_{\parallel,0}c)\delta\epsilon = c^2(\delta\boldsymbol{p}_{\perp})^2\,, \qquad (26)$$

where we took into account the two previous invariants that imply $\delta\epsilon = c\delta p_{\parallel}$. Now because $p_{\perp,0}$ is small, this constraint allows large variations of the polar angle of $\boldsymbol{p}_{\perp}$. Thus the variations of the energy and momenta are bounded, except for the angle of the transverse momentum that can vary randomly over the interval $(0, 2\pi)$; those erratic variations of the angle can occur with the β_z contribution to the transverse equations of motions that opens the phase space with another degree of freedom. This will have consequences on spatial diffusion, as will be seen further on.

The transport properties are to depend on the particle momentum, and one may define a reference energy

$$\epsilon_\star \equiv e\bar{E}'\ell_{\perp} \equiv a m_e c^2 \qquad (27)$$

As discussed before, $a/\gamma' \ll 1$ for supra-thermal particles, meaning that $\epsilon_\star \ll \epsilon$. Since these particles are strongly beamed toward the longitudinal direction, $\epsilon_0 \simeq p_{\parallel,0}c$ initially, and $p_{\perp,0}/p_{\parallel,0} \lesssim 1/\Gamma_{\rm s}$. In this limit, the transport of the supra-thermal particle can be described in configuration space as the random walk of a *non-relativistic* particle in the transverse plane, coupled to ballistic motion along the longitudinal direction. In the transverse plane, the particle is described as non-relativistic because its transverse velocity $\upsilon_{\perp} \simeq p_{\perp}/p_{\parallel}$ and, given that $\epsilon_\star \ll p_{\parallel,0}c$, the particle cannot exchange a large fraction of its parallel momentum with transverse momentum due to the invariance properties in this 2D approximation.

The transverse motion, devoid of linear resonance but governed by a continuum of Fourier modes, is thus characterized by a single nonlinear time

$$t_{\rm nl} \equiv \frac{\ell_{\perp}}{c}\left(\frac{2p_{\parallel,0}c}{\epsilon_\star}\right)^{1/2}\,. \qquad (28)$$

This is the time needed to cross a coherence cell for a particle that gets accelerated transversely in the transverse electric field. Over a coherence length, the electric field can be considered as constant and the particle receives a transverse kick $c\Delta p_{\perp} \sim \epsilon_\star$.

If the initial transverse momentum $p_{\perp,0} \ll \epsilon_\star/c$, the spatial transverse motion can be approximated by

$$\Delta\boldsymbol{x}_{\perp} \simeq \frac{1}{2}\frac{e\boldsymbol{E}_{\perp}}{p_{\parallel,0}}ct^2 + \boldsymbol{\upsilon}_{\perp,0}t\,, \qquad (29)$$

since the kick remains much smaller than $(\epsilon_\star p_{\parallel,0})^{1/2}$; $\boldsymbol{\upsilon}_{\perp,0} \equiv \boldsymbol{p}_{\perp,0}/p_{\parallel,0}$. The nonlinear time so defined is the time beyond which the nonlinear dynamics de-correlates the trajectories. It can also be considered as the time step for a random deflection of angle θ_i in the transverse plane since each crossing of a coherence cell in the transverse direction is associated to a large variation of θ_i when $p_{\perp,0} \ll \epsilon_\star/c$. Thus after n steps of size $\ell_{\perp}$, the trajectory has diffused such that

$$\langle\Delta\boldsymbol{x}^2_{\perp}\rangle \simeq \frac{1}{2}\ell^2_{\perp}n\,, \qquad (30)$$

with $n \simeq \Delta t/t_{\rm nl}$, which leads to a transverse spatial diffusion coefficient

$$D_{\perp} \simeq \frac{1}{4}\frac{\ell^2_{\perp}}{t_{\rm nl}} \propto p_{\parallel,0}^{-1/2}\,, \qquad (31)$$

where the numerical prefactor is subject to uncertainty.

If $p_{\perp,0}c \gg \epsilon_\star$, the transverse velocity undergoes small variation of its modulus in the crossing of a coherence cell, but it can undergo significant angle variations. This transverse quasi scattering can be analyzed in two regimes: (a) when $p_{\perp,0}c \ll (\epsilon_\star p_{\parallel,0})^{1/2}$ and (b) when $p_{\perp,0}c \gg (\epsilon_\star p_{\parallel,0})^{1/2}$ but still $p_{\perp,0} \ll p_{\parallel,0}$. In the former

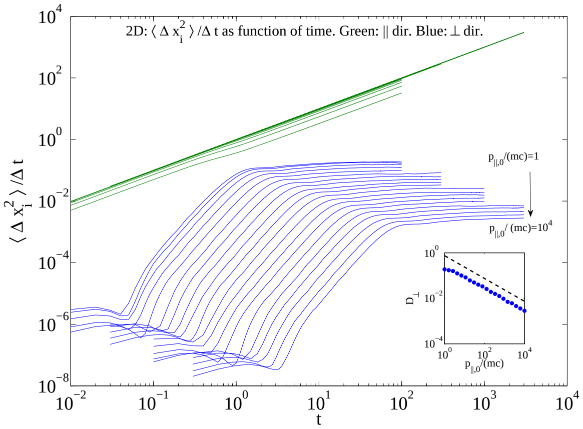

Figure 1. Time evolution of spatial diffusion coefficients for different $p_{\parallel,0}/(mc)$ in 2D fields geometry approximation. Green curves: parallel direction; Blue curves : transverse direction $[(x,y)$ plane]. Displacements in the parallel direction are clearly ballistic: $\langle \Delta x_\parallel^2 \rangle = \upsilon_{\parallel,0}^2 t^2$. In the transverse plane, at least two regimes are identified: when $t < t_{\rm nl}$, $\langle \Delta x_\perp^2 \rangle \propto t^4$ as expected from particle acceleration by nearly constant electric field over its coherence cell; and when $t > t_{\rm nl}$, $\langle \Delta x_\perp^2 \rangle/\Delta t$ reaches a plateau (i.e. diffusion) and its value has a power-law dependence on $p_{\parallel,0}$ with a slope of $-1/2$ (see subpanel). Subpanel: Transverse diffusion coefficient (plateau) dependence on initial particle momentum $p_{\parallel,0}$. Dashed line follows the power-law slope $-1/2$.

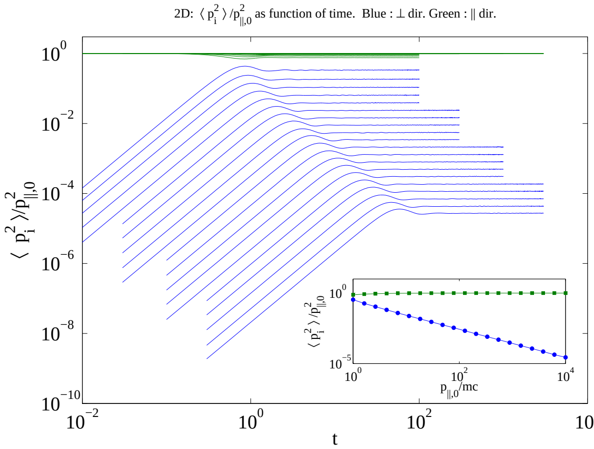

Figure 2. Time evolution of $\langle p_i^2 \rangle / p_{\parallel,0}^2$ for different values of $p_{\parallel,0}/(mc)$, in 2D approximation. Green curves: parallel (z) direction; Blue curves : transverse direction. Subpanel: Asymptotic values of $\langle p_i^2 \rangle / p_{\parallel,0}^2$ as function of $p_{\parallel,0}$. $\langle p_\parallel^2 \rangle / p_{\parallel,0}^2$ is slightly inferior to 1 independently from $p_{\parallel,0}$ (green squares). In transverse direction (blue circles) $\langle p_\perp^2 \rangle / p_{\parallel,0}^2 \propto p_{\parallel,0}^{-1}$.

limit, the particle crosses a transverse coherence cell in a nonlinear time scale as previously, whereas in the latter case the crossing occurs on a linear timescale $\ell_\perp/|\upsilon_\perp|$. Let us estimate the transverse diffusion coefficient for both cases. In case (a), when crossing a coherence cell, the particle undergoes a small transverse deflection of angle $\theta_i \sim \epsilon_\star/p_\perp c$. The scattering time is therefore longer than $t_{\rm nl}$ with $t_{\rm scatt} \sim \theta_i^{-2} t_{\rm nl}$ and diffusion in the transverse plane during $\Delta t > t_{\rm scatt}$ is such that

$$\langle \Delta \boldsymbol{x}_\perp^2 \rangle \sim \frac{\ell_\perp^2}{2} \left(\frac{t_{\rm scatt}}{t_{\rm nl}} \right)^2 \frac{\Delta t}{t_{\rm scatt}} \ . \tag{32}$$

This indicates that, in this regime of small deflection, a particle travels over a much larger distance than $\ell_\perp$ during a scattering time, namely $(t_{\rm scatt}/t_{\rm nl})\ell_\perp$. The transverse diffusion coefficient is thus

$$D_\perp \sim \frac{1}{4} \frac{\ell_\perp^2}{t_{\rm nl}} \left(\frac{p_\perp c}{\epsilon_\star} \right)^2 \ . \tag{33}$$

In case (b), the small deflection that occurs during the linear correlation time leads to a scattering time $t_{\rm scatt} \sim \theta_i^{-2} \ell_\perp/\upsilon_\perp$. And the transverse diffusion coefficient becomes:

$$D_\perp \sim \frac{1}{4} \upsilon_\perp \ell_\perp \left(\frac{p_\perp c}{\epsilon_\star} \right)^2 \ . \tag{34}$$

3.2 Numerical results in 2D-approximation

The system of equations of motions in the fields is solved by the Bulirsch-Stoer algorithm (Press et al. 1986), together with statistics over a sample of random phases and polarization directions of plane waves. The field $\boldsymbol{E}'_\perp$ is decomposed in plane waves with the constraint $\boldsymbol{k}' \parallel \boldsymbol{E}'_\perp$, which implies that $\boldsymbol{k}'$ is in the plane (x,y), choosing as before the normal direction along the $z-$direction. In this subsection we set $k'_z = 0$ and $E'_z = 0$ in the wave frame. Several hundreds of modes are used in the setting construction. The system converges quite rapidly with $\sim 10^3$ particles. For simplicity we investigate only the case were the initial particle momentum is oriented along the parallel direction, $\boldsymbol{p}_0 = p_{\parallel,0}\boldsymbol{e}_z$.

All simulations use the following units: the spatial length unit is $mc^2/(eE'_{\rm rms})$ ($E'_{\rm rms}$ is the root mean square of the electric field strength), the time unit is $mc/(eE'_{\rm rms})$, and momenta are expressed in units of mc. The coherence length $\ell_\perp \sim 1$ in these units.

Numerical results are presented in Figures 1,2. Fig. 1 depicts the time evolution of spatial diffusion coefficients for different $p_{\parallel,0}/(mc)$ in a 2D approximate geometry. Green curves depict the time evolution in the parallel direction and blue curves represent the same quantity in the transverse direction. Displacements in the parallel direction are clearly ballistic: $\langle \Delta x_\parallel^2 \rangle = \upsilon_{\parallel,0}^2 t^2$. In the transverse plane, at least two regimes are identified: for $t < t_{\rm nl}$, $\langle \Delta x_\perp^2 \rangle \propto t^4$ as expected from particle acceleration by nearly constant electric field over its coherence cell, see Eq. 29; for $t > t_{\rm nl}$, $\langle \Delta x_\perp^2 \rangle/\Delta t$ reaches a plateau (i.e. diffusion) and its value has a power-law dependence on $p_{\parallel,0}$ with slope of $-1/2$ (see the sub-panel of the figure), which fits well the result of the previous Section, see Eq. 31. This behavior is a direct consequence of particle trapping in every coherence cell it encounters, with a "waiting time" per cell being equal to $t_{\rm nl}$. The case where $p_{\perp,0}$ is different from zero was also investigated. In this case there is no more trapping in the field coherence cell but random motions in the transverse plane. We obtain a diffusive behavior on longer time-scales as discussed in the previous Section (e.g Eqs. 32, 33).

Figure 2 presents the evolution of $\langle p_\parallel^2 \rangle / p_{\parallel,0}^2$ (green curves) and $\langle p_\perp^2 \rangle / p_{\parallel,0}^2$ (blue curves) as function of time for different $p_{\parallel,0}/(mc) \in [1, 10^4]$. There is no diffusion in momentum space with parallel component being bounded by the π_z invariant, while the transverse one varies as $\langle \Delta p_\perp^2 \rangle/(mc)^2 \propto p_{\parallel,0}$. As generalized momentum is constrained by this π_z invariant, we expect a transverse momentum gain $\langle \delta p_\perp^2 \rangle = eE'_\perp \ell_\perp p_{\parallel,0}/c$.

Finally, we can mention that the energy gain $\langle \Delta\gamma \rangle$ is independent of $p_{\parallel,0}$ and corresponds to the amount of energy brought by the rms electric field potential. It can be expressed as $\langle \Delta\gamma \rangle = eE'_\perp \ell_\perp$. The energy variation from $\epsilon(p_{\parallel,0})$ to $\epsilon(p_{\parallel,0}) + qE'\ell_\perp$ takes place when $0 < t < t_{\rm nl}$. For $t > t_{\rm nl}$, the particle energy remains constant.

3.3 Transport in 3D-fields

We consider now the particle transport over a longer time with motions in the z direction, which involves the single resonant mode with $k_z = \delta_e^{-1}$ in the case of OTSI and a continuum of small wave numbers in the case of Weibel modes. In the wave frame, the longitudinal coherence length $\ell'_{\|} \simeq \gamma_{\rm m}\ell_{\|}$, and $\ell_{\|} \sim \ell_{\perp}$ for OTSI modes in the background plasma frame, so that $\ell'_{\|} \simeq \gamma_{\rm m}\ell'_{\perp}$. For Weibel modes, $\ell_{\|} > \ell_{\perp}$ and therefore $\ell'_{\|}/\ell'_{\perp} > \gamma_{\rm m}$.

The invariance of the generalized z-momentum is now broken and the particle momentum can diffuse in all directions. One limitation is the phase-space confinement due to the total energy conservation, that forbids energy diffusion. Another is that the longitudinal coherence length is significantly larger than the coherence length in the transverse direction. With respect to the above 2D analysis, we thus expect a change of regime when the motion in the z direction is felt by the particle, which occurs on time scales much larger than $\ell'_{\|}/c$, when a particle has crossed many coherence cells along the z-direction. The randomization of the longitudinal component of the momentum is expected over a time t_z, with

$$t_z \simeq \frac{\ell'_{\|}}{c}\left(\frac{p_{\|,0}c}{eE'_z\ell'_{\|}}\right)^2 \simeq \frac{\ell'_{\|}}{\ell'_{\perp}}\frac{\ell'_{\perp}}{c}\left(\frac{p_{\|,0}c}{\epsilon_\star}\right)^2 . \tag{35}$$

For both OTSI and Weibel modes, $E'_z\ell'_{\|} \simeq E'_{\perp}\ell'_{\perp}$ because in the wave frame, $\boldsymbol{\nabla}\times\mathbf{E}' = 0$. The above is a linear estimate of the scattering timescale in the longitudinal direction, however simulations at low energies suggest that the dependence on $\ell'_{\|}$ differs from this latter We will take into account that lack of knowledge by introducing a factor χ measuring the delay, compared to the 2D correlation time, in the full development of the 3D-dynamics. It will turn out to be important for the performance of the acceleration processes.

Over intermediate timescales, we expect to recover the previous results about the transverse diffusion and no diffusion in the longitudinal direction. But on time scale longer than t_z, one expects a 3D diffusion with

$$\begin{aligned} D_{\perp} &= \frac{1}{3}\ell'_{\perp}c\left(\frac{p_{\|}c}{\epsilon_\star}\right)^2 \\ D_{\|} &= \frac{\ell'_{\|}}{\ell'_{\perp}}D_{\perp} . \end{aligned} \tag{36}$$

As before we assumed that the deflection over a coherence cell is small with $\delta\theta \sim \epsilon_\star/p_{\|,0}c$. The description of the expected behaviors of these diffusion regimes is provided in the figures shown in the next paragraph.

3.4 Numerical results in 3D-fields

We take the same configuration as in the 2D case but with a finite value of $E'_{\|} = E'_{\perp}/\gamma_{\rm m}$ in the case of OTSI, with $k'_{\|}/k'_{\perp} = 1/\gamma_{\rm m}$. To simulate a Weibel turbulence, we include an ensemble of modes, consistent with the original wave equations of Weibel modes,

$$E'_{\|}(k'_{\|}) = -\frac{k'_{\|}}{k'^2_{\perp}}(\boldsymbol{k}'_{\perp}\times\boldsymbol{B}'_{\perp})\cdot\boldsymbol{\beta}_{\rm m} , \tag{37}$$

which insures the conservation of the total energy of each particle. For this ensemble of Weibel modes, $k'_{\|}/k'_{\perp}$ takes small values up to some parameter $\kappa < 1$; consequently, $E'_{\|}/E'_{\perp} \sim \kappa$. Most numerical calculations were done with the same time scales as in 2D case.

Figure 3 depicts the time evolution of spatial diffusion coefficients for different $p_{\|,0}/(mc)$ in 3D OTSI fields, assuming $\gamma_{\rm m} = 30$. Green curves correspond to the parallel direction and blue curves to the transverse direction. Displacements in parallel direction remain ballistic on numerical time scales and in transverse direction 2D-like diffusive behavior (see Fig. 1) disappears gradually when $t_{\rm nl} < t < t_z$. It will be seen further that the diffusive behavior is recovered in all directions on longer time scales (i.e. $t \gg t_z$). Figure 4 presents the evolution of $\langle p_i^2\rangle/p_{\|,0}^2$ in time for $p_{\|,0}/(mc) \in [1, 10^4]$. Comparing to Fig. 2, one observes that $\langle p_{\|}^2\rangle/p_{\|,0}^2$ keeps the same behavior as in 2D and the transverse components begin to rise at later times; longer time simulations are needed to explore its asymptotic behavior. Interestingly, a different behavior is observed for particles with momenta satisfying $t_{\rm nl} > t_{\|,\rm c}$: in this 3D OTSI turbulence, electromagnetic fields reverse every half coherence length along the longitudinal direction, due to the periodicity in that direction; therefore particles with $t_{\rm nl} > t_{\|,\rm c}$ execute oscillations in the transverse direction, with ballisitic motion along the longitudinal direction. Such particles are then confined in the transverse plane because their motion is reversed before they have time to experience a decorrelated field in the transverse plane. This is particularly important with respect to acceleration efficiency, since such particles would not return on a short timescale (in the absence of a mean field, of course). One can check that the condition $t_{\rm nl} > t_{\|,\rm c}$ amounts to $p_{\|,0} > \epsilon_\star\gamma_{\rm m}^2/2$ for $p_{\perp,0} = 0$, which is easily satisfied, or in terms of initial transverse velocity, $p_{\perp,0}/p_{\|,0} < 2/\gamma_{\rm m}^2$, which is also generically satisfied for the supra-thermal particles. This means that OTSI turbulence is inefficient from the point of view of scattering suprathermal particles away from the longitudinal direction.

In order to make an assessment of our estimates from subsection 3.3, a simulation with enhanced integration time was performed in the case where $p_{\|,0}/mc = 1$. The result is presented in Fig. 5 where different statistical quantities are plotted as a function of time. A slightly smaller value $\gamma_{\rm m} = 10$ is adopted here to reduce the characteristic t_z time. On time scales larger than t_z the spatial diffusion is recovered in all directions, all momenta are isotropized and energy gain is equal to the field rms energy. Note that the ratio between spatial diffusion coefficients in the parallel and transverse directions is not equal to $\gamma_{\rm m}$ as expected in Eq. 35: its value is $55 > \gamma_{\rm m}$ and scales as $0.6\gamma_{\rm m}^2$ when $\gamma_{\rm m}$ is varied explicitly in our simulations. It remains uncertain if this scaling depends on the choice of too low energy particles ($p_{\|,0}/(mc) = 1$) and if it remains the same for highest energies. Direct simulations for the former case, with large enought integration time, are numerically prohibive and are subject to severe numerical errors. In the following, we encode this uncertainty in a parameter χ, such that $\chi = \gamma_{\rm m}$ if the linear value given by Eq. 35 were to apply, but $\chi \sim \gamma_{\rm m}^2$ as indicated by the simulations.

Finally, in the Fig. 6 we present also the same simulation but in the case of 3D Weibel-type fields with $k'_{\perp}/k'_{\|} = 10$, corresponding to $\kappa = 0.1$. The general behaviour is similar to that observed for transport in OTSI turbulence. In particular, one recovers a scaling $t_z \propto \kappa^{-2}$ and $D_{\|}/D_{\perp} \propto \kappa^{-2}$ instead of the linear estimates given in Eqs. 35 and 36, which suggest a scaling in κ^{-1}. As before, we encode this uncertainty with a factor χ, so that $D_{\|}/D_{\perp} \simeq \chi$, the simulations indicating $\chi \simeq \left(\ell'_{\|}/\ell'_{\perp}\right)^2$.

As expected, the energy does not undergo a diffusive behavior. After a limited gain, the particles keep a constant momentum. This is in agreement with theoretical predictions: stochastic acceleration is not seen, transverse heating is bounded, the energetic particle beam is broadened in the transverse direction, but the distribution remains anisotropic.

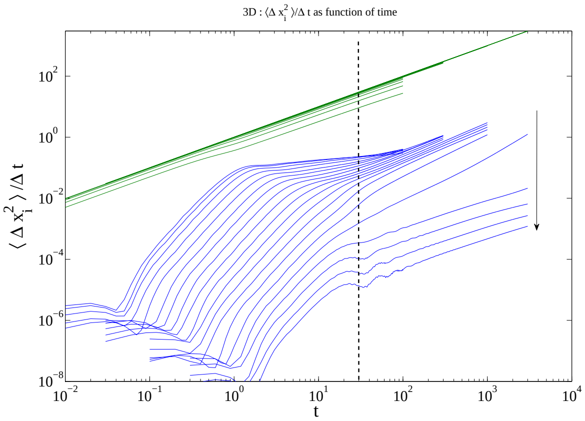

Figure 3. Transverse spatial diffusion in 3D modes of OTSI type. This graph depicts the time evolution of spatial diffusion coefficients for different $p_{\|,0}/(mc)$ in 3D fields. Green curves: parallel (z) direction; Blue curves: transverse direction $[(x, y)$ plane]. Dashed vertical line delimits the linear coherence time in z direction $t_{\|,c} = \gamma_{\rm m} l_\perp/c$. Displacements in the parallel direction remain ballistic on numerical time scales, since the integration time is too short to probe the diffusive behavior in this direction. In the transverse direction, 2D-like diffusive behavior (see Fig. [1]) disappears gradually when $t_{\rm nl} < t < t_z$.

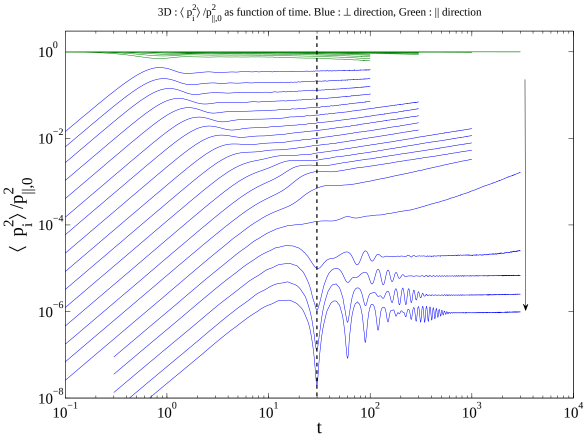

Figure 4. Time evolution of $\langle p_i^2\rangle/p_{\|,0}^2$ for different values of $p_{\|,0}/(mc)$, in 3D-fields. Green curves: parallel (z) direction; Blue curves: transverse direction. Dashed vertical line delimits the linear coherence time in z direction $t_{\|,c} = \gamma_{\rm m} l_\perp/c$. Comparing to the Fig. [2] $\langle p_\|^2\rangle/p_{\|,0}^2$ keeps the same behavior as in 2D and the transverse components begin to rise at later times but longer time simulations are needed to explore its asymptotic behavior. A different behavior are observed for particles with momenta satisfying $t_{\rm nl} > t_{\|,c}$, which are confined in a coherence cell in the transverse plane, see the text for details.

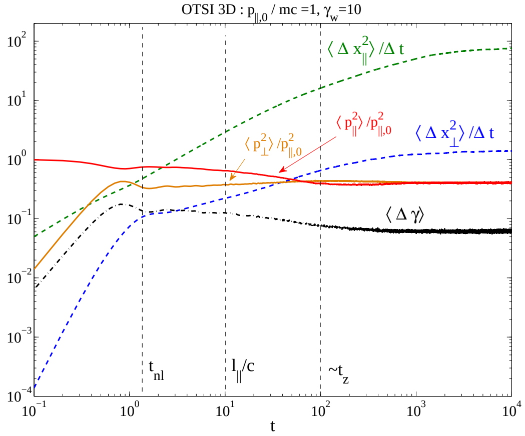

Figure 5. For OTSI modes, time evolution of different quantities in the case $p_{\|,0} = mc$ with enhanced integration time. Solid curves show the average $\langle p_i^2\rangle/p_{\|,0}^2$, red color for parallel direction and orange color for the transverse one. Dashed curves show spatial transport coefficients $\langle\Delta x_i^2\rangle/\Delta t$. Green color for parallel direction and blue for transverse direction. Dot-dashed black curve shows $\langle\Delta\gamma\rangle$. Vertical dashed lines indicate tree caracteristic times relevant for particle dynamics. As expected, spatial diffusion is present in all directions on time scales much longer than t_z. Above the diffusion time all momenta reach isotropy: $\langle p_x^2\rangle = \langle p_y^2\rangle = \langle p_z^2\rangle \simeq p_{\|,0}^2/3$.

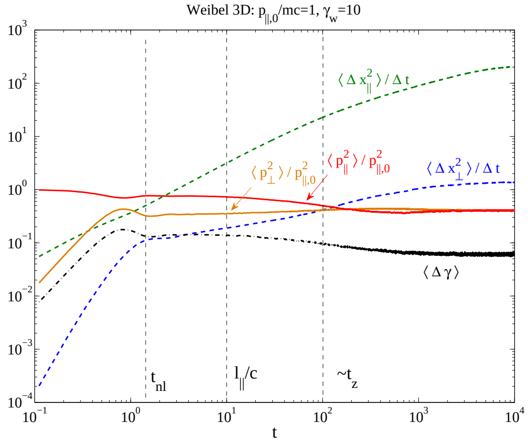

Figure 6. Same as in Fig. 5, but for Weibel 3D modes. Here, we take $k'_\|/k'_\perp = 1/10$. This choice is dictated by numerical time limitation in order to observe the development of a 3D regime. As expected, spatial diffusion is also present in all directions on time scales much longer than t_z. Above the diffusion time all momentum components reach isotropy: $\langle p_x^2\rangle = \langle p_y^2\rangle = \langle p_z^2\rangle \simeq p_{\|,0}^2/3$. We remark that the evolution is very similar to that obtained with OTSI modes, despite the finite range of k'_z wavenumbers.

4 ELECTRON HEATING

As we discussed in Section 2, the wiggler parameter for the background electrons in the proper frame of the micro-turbulent mode is very large, actually $a \gg \gamma'$, with γ' the typical Lorentz factor of the electrons in that frame. Since the modes carry a transverse electric field of the same order of the magnetic field, this offers a promising source of preheating in the shock precursor.

We first consider the effect of the electric field of the Weibel waves in their proper frame. The electron temperature temporarily increases, as long as their energy is smaller than $e\Delta\Phi' = e\bar{E}'_\perp\ell_\perp$, because, in this frame, the total energy of each particle is conserved, as discussed before for supra-thermal particles. This limiting energy is

$$\bar{\epsilon}' = e\bar{E}'_\perp\ell_\perp = \xi_{\rm B}^{1/2}\gamma_{\rm m}\frac{\ell_\perp}{\delta_{\rm i}}m_p c^2\ . \qquad (38)$$

Reverting to the background plasma frame, that energy corresponds to a temperature which is a sizeable fraction of the proton energy

$$T_{e,\lim} = \xi_{\rm B}^{1/2}\gamma_{\rm m}\frac{\ell_\perp}{\delta_{\rm i}}m_p c^2 \ , \tag{39}$$

assuming that most of the electron heating is distributed along the transverse direction. This transitory heating process is not in a diffusion regime, it is rather a direct linear acceleration in the coherent electric field of a coherent cell. Using Eq. 23, one can easily check that the energy $\overline{\epsilon'}$ is obtained over a typical linear timescale $\ell_\perp/c$. This fast heating in Weibel waves is a particular case of a situation where thermal electrons undergo strong relativistic motions in the waves, reaching relativistic temperatures $T_e \sim a\, m_e c^2$. A similar process is at work in the OTSI turbulence.

Because the transverse coherence scale is everywhere smaller than the precursor length scale, on which $\xi_{\rm B}$ varies, the above fast heating process brings forward a picture in which electrons are nearly instantaneously heated to the local temperature given by Eq. 39 above, scaling as $\xi_{\rm B}^{1/2}$. Of course, as the electrons near equipartition with the ions, one may expect the above heating process to saturate, notably because the oscillation parameter then becomes smaller compared to γ', as discussed in Sec. 2. Far from the shock, $\xi_{\rm B} \ll 1$ hence the electrons are heated to temperatures well below m_p/m_e (upstream frame), while closer to the shock, the temperature rises. Interestingly, the simulations of Sironi & Spitkovsky (2011a) indeed show a gradual evolution of the electron temperature over the length scale of the precursor. The above preheating process provides a concrete physical mechanism for this picture.

The previous estimate of the electron temperature allows to get a better knowledge of the filament size. The filament transverse equilibrium can be obtained from a simple pressure equilibrium argument, according to which: $\delta n T_e + \delta B^2/8\pi = 0$. This leads to

$$\xi_{\rm B} = 2\frac{|\delta n|}{n}\frac{T_e}{m_p c^2} \ , \tag{40}$$

and the existence of filaments implies a significant density trough such that $|\delta n|/n \sim 1$. Since

$$T_e = \xi_{\rm B}^{1/2}\gamma_{\rm m}\frac{\ell_\perp}{\delta_{\rm i}}m_p c^2 \ , \tag{41}$$

the coherence length and thus the filament size is such that $\ell_\perp \sim \gamma_{\rm m}^{-1}\xi_{\rm B}^{1/2}\delta_{\rm i}$ and the temperature

$$T_e \sim \xi_{\rm B} m_p c^2 \ ; \tag{42}$$

thus $\bar{\gamma}_e\mu \sim \xi_{\rm B}$ and the electron inertial scale (accounting for temperature) compares well with the coherence or filament radius:

$$\delta_e \sim \xi_{\rm B}^{1/2}\delta_{\rm i} \ . \tag{43}$$

The filament motion in the hottest phase is then determined through

$$\begin{aligned} \gamma_{\rm m} \quad &\sim \quad (\xi_{\rm cr}\xi_{\rm B})^{-1/4} \ \text{for close equipartition} \\ &\sim \quad \xi_{\rm cr}^{-1/2} \ \text{for } \xi_{\rm B} \leqslant \xi_{\rm cr} \ , \end{aligned} \tag{44}$$

which should thus increase with the distance to the shock.

Close to the shock front, the filament scale λ in the normal direction to get reflection is

$$\lambda \sim \frac{1}{\xi_{\rm B}^{1/2}\gamma_{\rm m}}\delta_{\rm i} \ , \tag{45}$$

so that

$$\lambda \quad \sim \quad \left(\frac{\xi_{\rm cr}}{\xi_{\rm B}}\right)^{1/4}\delta_{\rm i}$$

or

$$\lambda \quad \sim \quad \left(\frac{\xi_{\rm cr}}{\xi_{\rm B}}\right)^{1/2}\delta_{\rm i} \ , \ \text{for } \xi_{\rm B} \leqslant \xi_{\rm cr} \ . \tag{46}$$

If we furthermore postulate that λ corresponds to the efolding length scale $\ell_{\rm g} = \xi_{\rm cr}^{-1/2}\delta_{\rm i}$, then we find a simple relation between the two fundamental conversion factors: $\xi_{\rm B} \sim \xi_{\rm cr}^3$ in the first case, $\xi_{\rm B} \sim \xi_{\rm cr}^2$ in the second case. However the numerical works by Sironi & Spitkovsky (2011a) indicate a better performance of magnetic field generation with $\xi_{\rm B} \sim \xi_{\rm cr}$ in the case of a proton electron plasma; which suggests a steeper barrier: $\lambda \sim \delta_{\rm i}$. Only the cosmic rays fraction $\xi_{\rm cr}$ remains undetermined.

For background electrons this heating occurs in a very short time $\ell_\perp/c$, a few $\xi_{\rm cr}^{1/2}\omega_{\rm pi}^{-1}$, which is shorter than the growth time. The electron pre-heating has an important feedback on the instability. Although it does not saturate the instability, it reduces the phase velocity of the Weibel modes, at least because it increases the small mass ratio and determine the condition for the reflection of incoming protons.

Considering now OTSI modes, we have argued in section 4 that the heating process is similar, and we expect that it stops with the saturation of the OTSI when the electrons achieve a relativistic temperature.

So far, we have discussed the case of a nearly unmagnetized shock. One may recall that at high magnetization, the wake field develops in a p^+e^--plasma (Hoshino 2008, Lyubarsky 2006, Sironi & Spitkovsky 2011a). In the frame of the wake wave, there exists also an energy invariant that leads to a relativistic temperature for the electrons, but not to acceleration.

Across the shock front, the proton heating follows from the mixing of the different proton flows carrying energy of order $\Gamma_{\rm s} m_p c^2$ in front frame. More puzzling is the issue of electron heating. In the previous paragraph we saw that a significant preheating of the electron is expected. The final stage of electron heating across the shock front is necessarily related to an effective Joule effect due to scattering. The scattering frequency of thermal particles in the shocked flow is $\nu_{\rm s*} \sim \xi_{\rm B}\omega_{\rm pi}$ and the magnetic diffusivity $\nu_{\rm m} = \eta c^2/(4\pi) = \nu_{\rm s*}\delta_{\rm i}^2 \sim \xi_{\rm B} c\delta_{\rm i}$. The typical length of Joules dissipation is thus $\ell_{\rm J} = 3\nu_{\rm m}/c \sim 3\xi_{\rm B}\delta_{\rm i}$, which is a quite short distance for particle thermalization. A more detailed estimate is obtained by looking at the absorption of each Fourier mode, which leads to $\ell_{\rm J}(\lambda) = 3\lambda^2/\xi_{\rm B}\delta_{\rm i}$. All the magnetic energy that has been generated in the precursor is thus dissipated in the electron heating, the electron temperature remains in sub-equipartition with that of protons, $T_e \sim \xi_{\rm B}\Gamma_{\rm s} m_p c^2$. It turns out that both processes, pre-heating and Joules heating, have a similar contribution to the electron temperature.

Finally we have the estimates of all the scales involved in this physics, measured in the ambient frame they are:

- The Weibel instability growth length: $\delta_{\rm i}/\xi_{\rm cr}^{1/2}$
- The background electron heating scale: $\xi_{\rm cr}^{1/2}\delta_{\rm i}$
- The transverse scale of maximum instability in the hot phase: $\delta_e \sim \xi_{\rm B}^{1/2}\delta_{\rm i}$
- The transverse coherence length $\ell_\perp$, also the filament radius: $\ell_\perp \sim \xi_{\rm B}^{1/2}\delta_{\rm i}$
- The filament length: $\lambda \sim \delta_{\rm i}/\xi_{\rm cr}^{1/2}$ if $\xi_{\rm B} \sim \xi_{\rm cr}^2$; $\lambda \sim \delta_{\rm i}$ with $\xi_{\rm B} \sim \xi_{\rm cr}$.

5 APPLICATION TO ACCELERATION AT A GAMMA-RAY BURST EXTERNAL SHOCK

Section 3 provides the tools required to discuss the residence time of particles upstream of a relativistic shock. As discussed in Pelletier et al. (2009), one must compare the diffusion timescale in the micro-turbulence with the timescale associated to rotation in the background field and keep the shorter of the two. Let us discuss here the implications of the micro-turbulence. The Weibel filaments are likely the best sites of scattering, since the OTSI modes, at least in their linear description, lead to confinement of high energy particles along the shock normal.

The residence time of supra-thermal particles returning from the shocked plasma in the upstream flow is that corresponding to a deflection of an angle $1/\Gamma_{\rm s}$ after which the shock front catches it up again, and this fixes the acceleration time of the Fermi process. This has to be estimated in the filament frame first, in which the angle is $1/\gamma_{\rm f|m}$, with $\gamma_{\rm f|m}$ the relative Lorentz factor between the shock front and the wave frame, as determined by Eq. 9. The influence of a possible background magnetic field on the return timescale is discussed further below. For a particle of energy $\epsilon_{\rm m}$ in this wave frame, the residence time is

$$t_{\rm res,m} \sim \chi \frac{\ell_\perp}{c}\left(\frac{\epsilon_{|\rm m}}{\epsilon_\star}\right)^2 \frac{1}{\Gamma_{\rm f|m}^2}\ , \tag{47}$$

where χ is a factor large compared to unity. It accounts for the fact that the decorrelation time in the longitudinal direction is much larger than that in the transverse direction, as discussed above. For OTSI modes, the simulations indicate $\chi \sim \gamma_{\rm m}^2$, although the confinement in the transverse plane leads to very ineffective scattering; scattering is rather provided by the Weibel modes, for which $\chi \sim \gamma_{\rm m}^2 k_\perp/k_\parallel > \gamma_{\rm m}^2$, in terms of the wavenumbers of the instability measured in the background plasma rest frame.

Going to the front frame, one finds a residence timescale

$$t_{\rm res,f} \sim \chi \frac{\ell_\perp}{c}\left(\frac{\epsilon_{|m}}{\epsilon_\star}\right)^2 \frac{1}{\Gamma_{\rm f|m}^3}\ , \tag{48}$$

with $\epsilon_\star = (\gamma_{\rm m}/\Gamma_{\rm s})e\bar{B}_{|\rm f}\ell_\perp$ in terms of the turbulent magnetic field in the front frame $\bar{B}_{|\rm f}$, and $\epsilon_{|\rm f} \simeq \Gamma_{\rm f|m}(1-\beta_{\rm f|m})\epsilon_{\rm m}$.

$$t_{\rm res|f} \sim \chi \frac{\ell_\perp}{c}\left(\frac{\epsilon_{|\rm f}}{e\bar{B}_{|\rm f}\ell_\perp}\right)^2 \frac{\Gamma_{\rm s}}{\gamma_{\rm m}}\ . \tag{49}$$

The fact that the scattering takes place in a frame moving at high speed shortens the residence time, but this gain is mitigated by the anisotropy of the turbulent modes, which induces the χ factor.

5.1 Electron acceleration at relativistic shocks and radiation (GRBs)

We have developed arguments in favor of an efficient heating of the electron fluid by the micro-turbulence, which confirms the idea that the electrons could likely reach a sub-equipartition temperature at relativistic shocks. For instance in GRB termination shocks that give rise to the afterglow emission, they could achieve a temperature of a few tens of GeV. Indeed the proton temperature is very high at the beginning of the afterglow, and we have

$$T_e \lesssim T_p = \frac{\Gamma_{\rm s}}{3\sqrt{2}} m_p c^2\ ; \tag{50}$$

which corresponds to a few tens of GeV. Intense short scale magnetic turbulence develops because the interstellar magnetization parameter is very low, $\sigma \sim 10^{-9}$.

What kind of radiation can be expected in such small scale field, much more intense than the mean field? This depends on the wiggler parameter a, now measured in the downstream frame:

$$a \equiv \frac{e\bar{B}\ell_{\rm c}}{m_e c^2} \sim \xi_{\rm B}^{1/2}\Gamma_{\rm s}\frac{m_p}{m_e}\ . \tag{51}$$

This parameter measures the capability of the magnetic force to deviate a relativistic electron of Lorentz factor γ by an angle $1/\gamma$ (this is the reason for which γ does not appear in the definition). When $a > 1$ the magnetic field produces a single deviation of the electron in the emission cone of half angle $1/\gamma$, whereas when $a < 1$ the electron can undergo several wiggles in the emission cone. When a is large, the emission behaves like a normal synchrotron radiation in a mean field, except that there is no polarization. When a is small, the emission is of jitter type (Medvedev 2000). In the present case, the large wiggler parameter ensures that the emission caused by shocked and accelerated electrons at a relativistic shock is synchrotron-like; the analysis of the emitted spectrum may provide a diagnosis of the magnetic turbulence although the departures are expected to be moderate (e.g. Kirk & Reville 2010; Reville & Kirk 2010; Fleishman & Urtiev 2010; Medvedev et al. 2011) and likely dominated by the decay dynamics of the microturbulence downstream, which imply that particles of different Lorentz factors cool in regions of different magnetic field strengths (Lemoine 2012).

As for the supra-thermal electrons, we find a similar estimate of the maximum Lorentz factor, measured at shock front, achieved against synchrotron loss than the one derived by Kirk & Reville (2010) when $\gamma_{\rm m} \sim \Gamma_{\rm s}$, except of the dependence in $\gamma_{\rm m}$:

$$\begin{aligned}\gamma_{\rm max} \quad &\sim \quad \left(\frac{4\pi e^2\ell_{\rm c}}{\sigma_T m_e c^2}\frac{\gamma_{\rm m}}{\chi\Gamma_{\rm s}}\right)^{1/3} \sim \left(\mu n r_e^3\right)^{-1/6}\left(\frac{\gamma_{\rm m}}{\chi\Gamma_{\rm s}}\right)^{1/3} \sim \\ &\sim \quad 7\times 10^6\left(\frac{\gamma_{\rm m}}{\chi\Gamma_{\rm s}}\right)^{1/3}\ .\end{aligned} \tag{52}$$

To obtain this result we took into account the electron wandering upstream where it experiences a level of turbulence comparable to the downstream one, as measured in the front frame, because the extension of its trajectory upstream is much shorter than the high energy proton trajectories that shape the precursor. The corresponding maximum energy for the emitted photons received by an observer is

$$\begin{aligned}\epsilon_{\gamma,\rm max} \quad &\sim \quad \sqrt{\xi_{\rm B}}\frac{\Gamma_{\rm s}^{4/3}\chi^{-2/3}\gamma_{\rm m}^{2/3}}{(\mu n r_e^3)^{-1/6}}\frac{m_p c^2}{\alpha_f} \simeq \\ &\simeq \quad 3\times \xi_{\rm B,-2}^{1/2}\Gamma_{\rm s,2.5}^2 n_0^{1/2}\left(\frac{\gamma_{\rm m}}{\chi\Gamma_{\rm s}}\right)^{2/3}\ {\rm GeV}\ ,\end{aligned} \tag{53}$$

with the usual notation $\xi_{\rm B,-2} = \xi_{\rm B}/0.01$, $\Gamma_{\rm s,2.5} = \Gamma_{\rm s}/300$ and $n_0 = n/1\,{\rm cm}^{-3}$. This relatively high performance is due to the proton dynamics; otherwise with electron dynamics, only the MeV range would be reached.

The above estimate of $\gamma_{\rm max}$ balances the acceleration timescale against the timescale for synchrotron losses in the turbulent field. In principle, one should also include inverse Compton losses, which puts strict constraints on the return timescale in the upstream frame, as discussed by Li & Waxman (2006), Li & Zhao (2011). This requires to use the scattering timescale discussed above and follow the proper treatment of Klein-Nishina suppression given in these studies; this task is left for future work.

The above discussion considers an unmagnetized shock. In the presence of a background magnetic field, return in the upstream can be achieved through the rotation by an angle $1/\Gamma_{\rm s}$ in the background field. The return timescale then corresponds to $t_{\rm res,0|f} \sim \epsilon_{|\rm f}/(\Gamma_{\rm s} e B_0)$ as measured in the shock front frame, so that at the maximal Lorentz factor determined by Eq. 52

$$\frac{t_{\rm res,0|f}}{t_{\rm res|f}} \sim 2\left(\frac{\gamma_{\rm m}}{\chi}\right)^{2/3} \xi_{B,-2}B_{0,-5}^{-1}n_0^{2/3}\Gamma_{\rm s,2.5}^{1/3}\ , \tag{54}$$

with $B_{0,-5} = B_0/10\,\mu$G. This implies that the background magnetic field starts to dominate the dynamics of the highest energy electrons as soon as the ratio $\gamma_{\rm m}/\chi$ becomes significantly smaller than unity, for the above fiducial values. Among others, this guarantees that GeV photons can be produced, independently of $\gamma_{\rm m}/\chi$.

Thus a single synchrotron-like spectrum extending up to several GeV, even possibly a few tens, can be expected and thus is compatible with observations. From that point of view, the performance of relativistic shocks for electron acceleration and radiation can be regarded as quite high. The conversion factor into radiation is $\xi_{\rm rad} \sim \xi_{\rm B}\sigma_{\rm T} n r_{\rm s}\langle\gamma_e^2\rangle$ ($r_{\rm s}$ the external shock radius), and at the beginning of the afterglow $\xi_{\rm rad} \sim \xi_{\rm B} \sim 10\%$.

5.2 Relativistic shock and supra-thermal protons in GRBs

As mentioned previously, because the scattering time and thus the acceleration time increase with ϵ^2, the Fermi process at relativistic shocks is not expected to be an efficient accelerator of protons towards the highest energies. That acceleration is limited by expansion losses of time scale $r_{\rm s}/c$ in observer frame. At the termination shock of GRBs at the beginning of the afterglow, the maximum energy achieved when the residence time upstream balances the expansion time, is

$$\begin{aligned} E_{\rm max} &= 2Z\Gamma_{\rm s}\left(\frac{\gamma_{\rm m}}{\chi}\right)^{1/2}\xi_{\rm B}^{1/2}\sqrt{\frac{r_{\rm s}}{\delta_{\rm i}}}\,m_p c^2 \\ &\sim 3.7\times10^{15}\times Z\left(\frac{\gamma_{\rm m}}{\chi}\right)^{1/2}\Gamma_{\rm s,2.5}r_{\rm s,17}n_0^{1/4}\ eV\,. \qquad (55)\end{aligned}$$

Again, the above holds for an unmagnetized shock. The performance can be improved if one takes into account a background magnetic field, which leads to regular rotation and a shorter return timescale at these energies. The maximum energy can then be written $E_{\rm max,0} = Z\Gamma_{\rm s} e B_0 r_{\rm s} \sim 0.3\times10^7\times Z\,$GeV. Thus although an energy of order 10^{16} eV is achieved, the result is far from the range of so-called ultra-high energy cosmic rays.

6 ABOUT THE ORIGIN OF UHE-COSMIC RAYS

Precise performances of mildly or sub-relativistic shocks are not yet known and require more numerical simulations. However some reasonable guess are permitted by extrapolating what we know about the two extremes: non-relativistic and ultra-relativistic shocks. The main guess is that we can expect a magnetic field amplification at shocks with a conversion factor $\xi_{\rm B} = 1 - 10\%$, occurring in MHD regime (Bell 2004) without severe limitation due to the super-luminal configuration, especially for oblique internal shocks (termination shocks in the hot spots of FR2 jets might be super-luminal). These assumptions can be applied to internal shocks of AGN jets (in particular in Blazars jets), and to internal shocks of GRBs; the limitation of the acceleration of protons and nuclei is essentially the escape of particles at the edge of the flow. For a relativistic jet of radius r_j, with a large bulk Lorentz factor Γ_j and a kinetic power $P_{\rm jet} \simeq \rho_0 c^3\Gamma_j^2\pi r_j^2$ (ρ_0 being the co-moving density), the maximum energy given by assuming acceleration at the Bohm limit, i.e. an acceleration timescale $t_{\rm acc} = r_{\rm L}/c$ in the co-moving frame, the maximum energy in the observer frame reads (in agreement with Lemoine & Waxman 2009):

$$E_{\rm max} \simeq \Gamma_j Z e\bar{B} r_j \simeq Z\times10^{19}\left(\frac{\xi_{\rm B}}{10^{-2}}\,\frac{P_{\rm jet}}{10^{45}\,{\rm erg/s}}\right)^{1/2}\ {\rm eV}\,. \qquad (56)$$

Here we assumed that $\Gamma_{\rm s} \simeq 1$ so that $\bar{B}^2/4\pi \simeq \xi_{\rm B}\rho_0 c^2$. Therefore it is quite valuable to consider mildly relativistic shocks in ultra-relativistic flows.

The jets of FR2 radiogalaxies have a power $P_{\rm jet} = 10^{44} - 10^{46}$erg/s, hence they might produce UHECRs (Ptuskin et al. (2011)). GRBs flows carrying internal shocks can be even more efficient accelerators, depending of the duration of the flow for a given energy. For instance, a GRB of apparent isotropic luminosity $P_{\rm jet}/(\theta_j^2/4) \sim 10^{52}$ erg/s (θ_j being the half opening angle of the flow $> 1/\Gamma_j$) with $\Gamma_j \sim 100$ may produce particles with energy as high as $Z\times10^{21}$ eV for a similar conversion factor $\xi_{\rm B} = 0.01$. Thus mildly or sub-relativistic shocks in a relativistic flow are more efficient accelerators of protons than ultra-relativistic shocks and are excellent candidates for being sources of UHECRs, thanks to the magnetic field amplification at shocks.

Now if we consider FR1-jets, they are less powerful than the FR2, with $P_{\rm jet} = 10^{42} - 10^{43}$ erg/s and they are sub-relativistic. The maximum energy achieved in those jets is at least one order of magnitude lower than that achieved in FR2-jets. In principle, this might be compensated by the generation of UHECRs in the form of iron nuclei (Z=26) (Aloisio at al. 2011). For instance, we have fairly precise VLBI measurement of the radius of Centaurus A at several distances from the nuclei, together with estimate of the magnetic field responsible for synchrotron emission; this leads to an estimate of the product $\bar{B}r_j \simeq 2\times10^{-3}$ G pc. The Hillas criterium leads to $E_{\rm max} \simeq Z\times2\times10^{18}$ eV (see Lemoine & Waxman 2009), which is consistent with a significant amplification of the magnetic field at internal shocks. The most recent VLBI map of Centaurus A, done by the TANAMI project (Müller et al. 2011), reveals structures in the flow, suggesting internal shocks. The recent data analysis of Pierre Auger Observatory suggests an enrichment of the UHECR spectrum with heavy elements at higher energies and also a possible correlation with Centaurus A. However it is very difficult to understand the observed pattern of anisotropy if one assumes that the observed particles are heavier than hydrogen (Lemoine & Waxman 2009). In this sense, a contribution of protons coming from more remote and more powerful sources appears unavoidable.

7 CONCLUSIONS AND PROSPECTS

The triangular dependence of collisionless shock structure with a reflecting barrier for a part of incoming particles, with generation of supra-thermal particles and the generation of magnetic turbulence is a successful paradigm that applies to astrophysical shocks, both non-relativistic and relativistic. Numerical and theoretical works are making significant progress for both understanding the physics and providing quantitative results useful for astrophysical investigations. This includes not only the spectrum index and cut off of the distribution of accelerated particles, but also the conversion factors into cosmic rays, magnetic turbulence and radiation. We are likely seeing only the beginning of such studies, that require more PIC simulations and new types of hybrid codes involving relativistic MHD coupled with PIC codes for cosmic rays.

In this paper we have presented new theoretical investigations, namely the crucial effect of the motions of magnetic disturbances, the detailed analysis of the contribution of OTSI and the issue of the pre-heating of background electrons. The electron preheating is insured by a motional electric field in the wave-frame, the intensity of this field is almost the same of the magnetic field. Particles experience scattering and heating at the same rate.

Despite that the Weibel instability generates magnetic filaments whereas OTSI generates almost electrostatic waves in the background plasma, they behave similarly in their proper frame, in which they are composed of an electro-static field and a magnetostatic field of almost the same amplitude. The supra-thermal particles scatter in these fields while the background electrons are pre-heated up to sub-equipartition in such fields, because they experience relativistic oscillations. The preheating is particularly efficient: within a coherence length of the perturbations, it heats the electrons to $\sim \xi_{\rm B} m_p c^2$, in which $\xi_{\rm B}$ should be understood as the local (position dependent) fraction of energy density stored in the electromagnetic component. Because the coherence length is much shorter than the size of the precursor, this brings forward the picture in which the electrons are instantaneously heated to the above temperature, so that their temperature rises gradually towards near equipartition as they approach the shock front, a picture which appears in satisfactory agreement with the results of Sironi & Spitkovsky (2009), Sironi & Spitkovsky (2011a).

Electron pre-heating modifies the generation of microturbulence: it saturates OTSI and slows down the propagation of Weibel modes. So we envisage that the nose of the precursor contains fast propagating Weibel modes and then, closer to the shock front, relativistic thermal electrons that quench OTSI, slow down Weibel modes, enlarge the characteristic scale. The reflection of incoming protons is made possible under that condition of hot electrons with an enhancement of magnetic energy density up to a fraction of ρc^2 over a distance of a few proton inertial scales $\delta_{\rm i}$. Thus the OTSI instability, although it grows a little faster than the Weibel instability, plays a transitory role in the precursor of an ultra-relativistic shock; although it plays a role similar to the Weibel instability, it saturates when the electrons become relativistically hot. The OTSI modes are probably not transmitted downstream, where they would propagate as electromagnetic waves of a quasi-vacuum. Nevertheless they are definitely active in the cold phase of the shock precursor, like Buneman instabilities that also preheat efficiently the electrons.

The motions of magnetic filaments relate to the 3D description of the modes, and the 3D description is crucial for the development of the scattering process. Clearly, because of the filament nature of these magnetic structures, the time scale for a full development of 3D scattering is essential. Indeed the performances of the acceleration process can be reduced significantly (as described by our factor χ) as the time required to reach 3D-scattering increases. The simulations (Spitkovsky 2008a, Sironi & Spitkovsky 2011a) of the Fermi process in 2D probably involves mirror effects on the shock front rather than actual upstream/downstream scattering, especially at the “low” energies corresponding to the first Fermi cycles probed by these simulations. To probe the 3D scattering regime discussed here, one would need 3D PIC simulations with very long integration timescales, in order to accelerate particles to energies such that their Larmor radius in the turbulent field becomes larger than the coherence length.

The combination of Weibel and OTSI turbulence can produce a kind of relativistic second order Fermi process upstream, in addition to the effect of their own electric field. However the interaction time is limited by the residence time of supra-thermal particles upstream; therefore a significant improvement of the acceleration process is doubtful.

Shocks in AGN, blazar jets, or in the internal flow of GRBs are mildly relativistic and therefore not subject to the severe restriction imposed to the Fermi process by the mean field like what happens in the ultra-relativistic termination shocks of pulsar wind nebulae and of gamma-ray bursts. In pulsar wind nebulae, reconnections likely contribute to injecting high energy particles in the shock and a supra-thermal tail with a hard component may be generated (Lyubarsky 2003; Pétri & Lyubarsky 2007; Sironi & Spitkovsky 2011b). In the termination shock of a GRBs, the magnetization is very weak and Fermi acceleration becomes operative when it decreases below some critical value, because the conditions for generating magnetic turbulence are fullfilled, as suggested by observations (Li & Waxman 2006; Li & Zhao 2011). When the termination shock propagates in a star wind whose density decreases like $1/r^2$, the Fermi process may be, in a first step, quenched by the mean field, if the magnetization is large; then as the magnetization decreases, it starts and generates very high energy electrons (Lemoine & Pelletier 2011b). When the shock propagates in a normal interstellar medium of very low magnetization, the Fermi process works at the very beginning. Fermi process at an ultra-relativistic shock is a very efficient accelerator of electrons, the scattering rate at low energy being very high. And because it generates also a very intense magnetic field at short scales thanks to the incoming proton energy, it produces a very intense and extended synchrotron-like spectrum up to GeV energies.

ACKNOWLEDGEMENT

It is a pleasure to acknowledge fruitful discussions with Lorenzo Sironi and Brian Reville, supported by ISSI. This work has been financially supported by the GdR PCHE and the GDRE ”Exploring the Dawn of the Universe with Gamma-Ray Bursts” and by the PEPS-PTI Program of the INP/CNRS.

REFERENCES

Achterberg, A., Gallant, Y., Kirk, J. G., Guthmann, A. W. 2001, MNRAS 328, 393

Achterberg, A. & Wiersma J., 2007, A & A, 475, 1

Aloisio R., Berezinsky V., Gazizov A., 2011, Astroparticle Phys., 34, 620

Bednarz, J., & Ostrowski, M. 1998, Phys. Rev Letters, 80, 3911

Bell, A. 2004, MNRAS, 353, 550

Bret, A., Firpo, M.-C., Deutsch, C. 2004, Phys. Rev. E, 70, 046401

Chang P., Spitkovsky A., Arons J., 2008, ApJ, 674, 378.

Ellison, D., & Double, G. 2002, Astroparticle Physics, 18, 213

Fainberg Y.B., Shapiro V.D., Shevchenko V.I., 1970, Sov. Phys. JETP, 30, 528.

G. D. Fleishman G.D., Urtiev F.A. 2010, MNRAS, 406, 644

Gallant, Y. A., & , A. 1999, MNRAS, 305, L6

Gallant, Y.A., Hoshino M., Langdon A.B., Arons J., Max C.E. 1992, ApJ, 391, 73.

Gedalin M., Smolik E., Spitkovsky A., Balikhin M., 2012, EPL, 97, 35002

Hoshino, M. 2008, ApJ, 672, 940

Hoshino, M., Arons J. 1991, Phys. Fluids B, 3, 818

Jones, F. C., Jokipii, J. R., Baring, M. C., 1998, ApJ, 509, 238

Keshet, U., Katz, B., Spitkovsky, A., Waxman E., 2009, ApJ, 693, L127

Kirk, J., Guthmann, A., Gallant, Y., & Achterberg, A. 2000, ApJ, 542, 235

Kirk J., Reville B. 2010, ApJ, 710, 16

Lemoine, M., Pelletier, G. 2003, ApJ, 589, L73

Lemoine, M., Pelletier, G., Revenu, B. 2006, ApJ, 645, L129

Lemoine, M., & Waxman, E. 2009, JCAP, 11, 9

Lemoine, M., Pelletier, G., 2010, MNRAS, 402, 321
Lemoine, M., Pelletier, G., 2011a, MNRAS, 417, 1148
Lemoine, M., Pelletier, G., 2011b, MNRAS, 418, L64
Lemoine, M., 2012, arXiv:1206.4187
Li, Z., Waxman, E. 2006, ApJ, 651, L328
Li, Z., Zhao, X.-H., 2011, JCAP, 05, 008
Lyubarsky, Y., 2003, MNRAS, 345, 153
Lyubarsky, Y., 2006, ApJ, 652, 1297
Martins, S. F., Fonseca, R. A., Silva, L. O., Mori, W. B., 2009, ApJ 695, L189
Medvedev M. V., Loeb A., 1999, ApJ, 526, 697
Medvedev, M. V. 2000, ApJ, 540, 704
Medvedev, M. V., Trier Frederiksen, J., Haugboelle, T., Nordlund, A., 2011, ApJ, 737, 55
Niemec, J., Ostrowski, M., Pohl, M. 2006, ApJ, 650, 1020
Müller et al., 2011, A & A, 530, 11
Pelletier G., Lemoine M., & Marcowith A. 2006, A & A, 453,181
Pelletier G., Lemoine M., & Marcowith A. 2009, MNRAS, 393, 587
Pétri, J., Lyubarsky, Y., 2007, A&A, 473, 683
Plotnikov I., Pelletier G., Lemoine M., 2011, A & A, 532, 68
Press W. H., Flannery B. P., Teukolsky S. A. , & Vetterling W. T. 1986, Numerical Recipes (Cambridge: Cambridge Univ. Press)
Ptuskin V.S., Rogovaya S.I., Zirakashvili V.N., 2011, astro-ph, arXiv:1105.4491
Rabinak I., Katz B., Waxman E., 2011, ApJ, 736, 157
Reville, B., Kirk, J. G., 2010, ApJ, 724, 1283
Shaisultanov R., Lyubarsky Y., Eichler D., 2011, astro-ph HE, arXiv:11040521.v1
Sironi, L., Spitkovsky, A. 2009, ApJ, 698, 1523
Sironi, L., Spitkovsky, A. 2011a, ApJ, 726, 75
Sironi, L., Spitkovsky, A. 2011b, ApJ, 741, 39
Spitkovsky, A., 2008, ApJ, 673, L39
Spitkovsky, A., 2008, ApJ 682, L5

APPENDIX A: WEIBEL INSTABILITY WITH A NON-VANISHING PARALLEL WAVENUMBER

Despite detailed analysis of the relativistic beam instability in Weibel regime, like for instance in Achterberg & Wiersma (2007), Shaisultanov et al. (2011), and Bret et al. (2005), the motion of filaments has not been given attention so far. We will emphasize this issue for cold and relativistically hot electron fluid.

For a cold background plasma pervaded by a cold beam, the wave system is described by the matrix:

$$\Lambda_{ij} = \left(1 - \frac{\omega_{\rm p}^2}{\omega^2}\right) - \frac{k^2c^2}{\omega^2}\left(\delta_{ij} - \frac{k_i k_j}{k^2}\right) + \chi^{\rm b}_{ij} \, , \tag{A1}$$

where $\chi^{\rm b}_{ij}$ are the components of the susceptibility tensor of the beam plasma given by

$$\chi^{\rm b}_{ij} = -\xi_{\rm cr}\mu\frac{\omega_{\rm pe}^2}{\omega^2}\left(\delta_{ij} + \frac{k_i\upsilon_j + k_j\upsilon_i}{\omega - \boldsymbol{k}\cdot\boldsymbol{\upsilon}_{\rm b}} + \frac{k^2c^2 - \omega^2}{(\omega - \boldsymbol{k}\cdot\boldsymbol{\upsilon}_{\rm b})^2}\frac{\upsilon_i\upsilon_j}{c^2}\right) \, . \tag{A2}$$

We chose a beam velocity direction along z-axis, $\boldsymbol{\upsilon}_{\rm b} = \upsilon_{\rm b}\boldsymbol{e}_z$ and a wave vector $\boldsymbol{k} = k_x\boldsymbol{e}_x + k_z\boldsymbol{e}_z$. Electromagnetic waves polarized in the y-direction are decoupled. The wave system of interest reduces to second order, such that

$$\begin{aligned}
\Lambda_{xx} &= 1 - \frac{\omega_{pe}^2}{\omega^2}\left(1 + k_z^2\delta_e^2 + \xi_{\rm cr}\mu\right) \\
\Lambda_{xz} = \Lambda_{zx} &= \frac{k_x k_z c^2}{\omega^2} - \xi_{\rm cr}\mu\frac{\omega_{\rm p\mathit{e}}^2}{\omega^2}\frac{k_x\upsilon_{\rm b}}{\omega - k_z\upsilon_{\rm b}} \\
\Lambda_{zz} &= 1 - \frac{\omega_{\rm pe}^2}{\omega^2}\left(1 + k_x^2\delta_e^2 + \xi_{\rm cr}\mu\right) \\
&\quad - \xi_{\rm cr}\mu\frac{\omega_{\rm pe}^2}{\omega^2}\left(\frac{2k_z\upsilon_{\rm b}}{\omega - k_z\upsilon_{\rm b}} + \frac{k^2c^2 - \omega^2}{(\omega - k_z\upsilon_{\rm b})^2}\beta_{\rm b}^2\right)
\end{aligned}$$

And the dispersion relation is

$$\mathcal{D}(k, \omega) = \Lambda_{xx}\Lambda_{zz} - \Lambda_{xz}^2 = 0 \tag{A3}$$

In the case of Weibel instability, $\omega^2 \ll \omega_{\rm pe}^2$, $k_x^2\delta_e^2 \sim 1$ and $k_z^2\delta_e^2 \ll 1$, we find:

$$\omega = k_z\upsilon_{\rm b}\left(1 - \xi_{\rm cr}\mu\frac{\gamma_{\rm b}^{-2} + k_\perp^2\delta_e^2}{1 + k_\perp^2\delta_e^2}\right) + i\sqrt{\xi_{\rm cr}\mu}\frac{k_\perp\upsilon_{\rm b}}{(1 + k_\perp^2\delta_e^2)^{1/2}} \, , \tag{A4}$$

with $k_\perp = k_x$. This is the result for a cold background plasma and a cold beam. When one takes into account a dispersion of the beam within an angle $1/\Gamma_{\rm s}$, as previously investigated (Rabinak et al. 2011; Lemoine & Pelletier 2011a), the instability is quenched when $\Gamma_{\rm s} < (\xi_{\rm cr}\mu)^{-1/2}$. However the instability is restored when the background electrons are sufficiently hot with both the same growth rate and the same frequency. In the case of OTSI, electron heating up to relativistic temperature tends to quench the instability because the modes become super-luminal and thus the resonant interaction is no more possible; this effect is however delayed by the fact that the frequency is negatively shifted by the beam, which lowers the phase velocity.

Let us now study Weibel's instability properties for a relativistic electron temperature. As the electrons can come close to equipartition, it is essential to account for the response of the background ions. Let us write the components of the wave tensor:

$$\begin{aligned}
\Lambda_{xx} &= \varepsilon_\parallel\frac{k_x^2}{k^2} + \left(\varepsilon_\perp - \eta^2\right)\frac{k_z^2}{k^2} + \chi^{\rm b}_{xx} \\
\Lambda_{xz} = \Lambda_{zx} &= \left(\varepsilon_\parallel - \varepsilon_\perp + \eta^2\right)\frac{k_x k_z}{k^2} + \chi^{\rm b}_{xz} \\
\Lambda_{zz} &= \varepsilon_\parallel\frac{k_z^2}{k^2} + \left(\varepsilon_\perp - \eta^2\right)\frac{k_x^2}{k^2} + \chi^{\rm b}_{zz}
\end{aligned} \tag{A5}$$

where the dielectric coefficients for relativistically hot electrons and cold protons in the low frequency approximation are:

$$\varepsilon_\parallel \simeq 1 - \frac{\omega_{\rm pi}^2}{\omega^2} + \frac{1}{k^2\lambda_{\rm De}^2}\left(1 + i\frac{\pi}{2}\frac{\omega}{kc}\right) \tag{A6}$$

$$\varepsilon_\perp \simeq 1 - \frac{\omega_{\rm pi}^2}{\omega^2} - \frac{1}{k^2\lambda_{\rm De}^2}\left(1 - i\frac{\pi}{4}\frac{kc}{\omega}\right) \tag{A7}$$

When considering relativistically hot electrons, it is convenient to write the Debye length λ_{De} such that

$$\lambda_{\rm De}^2 \equiv \frac{T_e}{4\pi ne^2} = \bar{\mu}\delta_{\rm i}^2 \text{ with } \bar{\mu} \equiv \frac{1}{3}\bar{\gamma}_e\mu \text{ and } \bar{\gamma}_e \equiv 1 + 3T_e/m_ec^2 \, .$$

Whereas the Landau contribution (imaginary part) is a small correction in the longitudinal response, it is dominant in the transverse response.

$$\begin{aligned}
\omega^2\Lambda_{xx} &= \omega^2\left(1 + \frac{\omega_{\rm pi}^2}{\bar{\mu}k^2c^2}\right) - \omega_{\rm pi}^2\left(1 + \xi_{\rm cr}\right) \\
\omega^2\Lambda_{xz} = \omega^2\Lambda_{zx} &= \frac{\omega^2}{k^2\lambda_{De}^2}\left(2 - i\frac{\pi}{4}\frac{kc}{\omega}\right)\frac{k_x k_z}{k^2} + k_x k_z c^2 \\
&\quad - \xi_{\rm cr}\omega_{\rm pi}^2\frac{k_x\upsilon_{\rm b}}{\omega - k_z\upsilon_{\rm b}}
\end{aligned}$$

$$\begin{aligned}\omega^2\Lambda_{zz} \quad &= \quad \omega^2\left(1-\frac{\omega_{\rm pi}^2}{\bar{\mu}k^2c^2}\right)+i\frac{\pi}{4}\frac{\omega_{\rm pi}^2}{\bar{\mu}}\frac{\omega}{kc}\\ &\quad -\omega_{\rm pi}^2\left(1+k_x^2\delta_{\rm i}^2+\xi_{\rm cr}+\xi_{\rm cr}\frac{2k_z\upsilon_{\rm b}}{\omega-k_z\upsilon_{\rm b}}\right.\\ &\quad \left.+\xi_{\rm cr}\frac{k^2c^2-\omega^2}{(\omega-k_z\upsilon_{\rm b})^2}\beta_{\rm b}^2\right)\end{aligned}$$

An important observation is that $\omega_{\rm pb} < \omega_{\rm pi}$, so that one can neglect $|\omega|^2$ in front $\omega_{\rm pi}^2$. Furthermore, at equipartition, the ions contribute strongly to the instability and the typical wavenumber $k_x \sim \omega_{\rm pi}$, whereas for $\bar{\mu} \ll 1$, the response of the electrons dominate, and $k_x \to \bar{\mu}^{-1/2}\omega_{\rm pi}$, the latter corresponding to the relativistic electron plasma frequency. Thus the dispersion relation can be written (omitting also a term in $\xi_{\rm cr}^2$, and assuming $k_z^2\delta_{\rm i}^2 \ll 1$):

$$\begin{aligned}&\left(1-\frac{\omega^2}{\bar{\mu}k^2c^2}\right)\left[-i\frac{\pi}{4}\frac{\omega}{\bar{\mu}kc}+1+k^2\delta_{\rm i}^2+\xi_{\rm cr}\left(\frac{k^2c^2}{\delta\omega^2}+\frac{2}{\gamma_{\rm b}^2}\frac{k_z\upsilon_{\rm b}}{\delta\omega}\right)\right]\\ &\qquad +2\xi_{\rm cr}\frac{k_z\upsilon_{\rm b}}{\delta\omega}\left(k_x^2\delta_{\rm i}^2-i\frac{\pi}{4}\frac{\omega}{\bar{\mu}kc}\frac{k_x^2}{k^2}\right)=0 \qquad \text{(A8)}\end{aligned}$$

We solve that equation by setting $\delta\omega = \nu + i\gamma$ with the approximation $|\nu| \ll |\gamma|$ (γ should not be confused with Lorentz factors appearing elsewhere). The growth rate is the positive root of the equation

$$\frac{\pi}{4}\frac{\gamma^3}{\bar{\mu}k^3c^3}+\left(1+k^2\delta_{\rm i}^2\right)\frac{\gamma^2}{k^2c^2}-\xi_{\rm cr}=0\ , \qquad \text{(A9)}$$

which gives

$$\gamma \ \simeq\ \sqrt{\xi_{\rm cr}}\upsilon_{\rm b}\omega_{\rm pi}\,\frac{k_x\delta_i}{[1+(k_x\delta_i)^2]^{1/2}}\ , \qquad \text{(A10)}$$

provided $(k_x\delta_i)^3 \gtrsim \sqrt{\xi_{\rm cr}}/\bar{\mu}$. If $\bar{\mu} > \sqrt{\xi_{\rm cr}}$, the latter inequality is verified for $k_x\delta_i \gtrsim 1$, which means the filamentation instability is of the ion-ion type, with typical wavenumber $k_x \sim \delta_i^{-1}$. If, however, $\bar{\mu} < \sqrt{\xi_{\rm cr}}$, the instability is pushed towards higher values of k_x, as the response of the hot electrons dominates.

The frequency shift is obtained at the first order of the expansion in ν:

$$\nu\ \simeq\ -k_z\upsilon_{\rm b}\frac{\frac{\pi}{8}\gamma+(k_x\delta_i)^3\bar{\mu}\xi_{\rm cr}\omega_{\rm pi}}{\frac{3\pi}{8}\gamma+(k_x\delta_i)\left[1+(k_x\delta_i)^2\right]\bar{\mu}\omega_{\rm pi}}\ . \qquad \text{(A11)}$$

Using the value of γ and simplifying $1 + (k_x\delta_i)^2 \sim (k_x\delta_i)^2$, one obtains

$$\nu\ \sim\ -k_z\upsilon_{\rm b}\sqrt{\xi_{\rm cr}}\frac{\frac{\pi}{8}+(k_x\delta_i)^3\bar{\mu}\sqrt{\xi_{\rm cr}}}{\frac{3\pi}{8}\sqrt{\xi_{\rm cr}}+(k_x\delta_i)^3\bar{\mu}}\ , \qquad \text{(A12)}$$

which takes different scalings, depending on the comparison between $\bar{\mu}$ and $\xi_{\rm cr}$.

If $\bar{\mu} > \sqrt{\xi_{\rm cr}}$, the filamentation instability grows at $k_x\delta_i \sim 1$, so that

$$\nu\ \sim\ -k_z\upsilon_{\rm b}\frac{\pi}{8}\frac{\sqrt{\xi_{\rm cr}}}{\bar{\mu}} \qquad \left(\bar{\mu} > \sqrt{\xi_{\rm cr}},\ k_x\delta_i \sim 1\right)\ . \qquad \text{(A13)}$$

If $\bar{\mu} < \sqrt{\xi_{\rm cr}}$, maximum growth takes place at $k_x\delta_i \simeq \bar{\mu}^{-1/2}$, so that

$$\nu\ \sim\ -k_z\upsilon_{\rm b}\left(\frac{\pi}{8}\sqrt{\bar{\mu}\xi_{\rm cr}}+\xi_{\rm cr}\right) \qquad \left(\bar{\mu} < \sqrt{\xi_{\rm cr}},\ k_x\delta_i \sim \bar{\mu}^{-1/2}\right)\ , \qquad \text{(A14)}$$

although it should be noted that the growth rate increases weakly with $k_x\delta_i$, and that the frequency shift evolves in a non-trivial way with k_x in the interval $\xi_{\rm cr}^{1/6}\bar{\mu}^{-1/3}\omega_{\rm pi} \to \bar{\mu}^{-1/2}\omega_{\rm pi}$.

We expect that the size of the Weibel filaments, i.e. the transverse coherence length is determined by the maximum k_x; thus $\ell_\perp \sim \delta_i\sqrt{\bar{\mu}}$ far from equipartition, with $\ell_\perp \to \delta_i$ close to equipartition. For this typical size, the filament Lorentz factor goes from $\gamma_{\rm m} \sim \xi_{\rm cr}^{-1/2}$ when $\bar{\mu} < \xi_{\rm cr}$ to $\gamma_{\rm m} \sim (\bar{\mu}\xi_{\rm cr})^{-1/4}$ when $\xi_{\rm cr} \lesssim \bar{\mu} \lesssim \sqrt{\xi_{\rm cr}}$, and to $\gamma_{\rm m} \sim \xi_{\rm cr}^{-1/4}\bar{\mu}^{1/2}$ for $\bar{\mu} > \sqrt{\xi_{\rm cr}}$.

The wave-length in the normal direction is limited by $k_z\upsilon_{\rm b} < \gamma$ which implies $\ell_\parallel > \delta_{\rm i}/\sqrt{\xi_{\rm cr}}$, which is comparable with the growth length.

APPENDIX B: CO-VARIANT TRANSPORT EQUATION FOR PLASMA MODES

We consider the transport equation of plasma modes with the right hand side involving the Einstein coefficients α and β, knowing that in case of an instability, $\beta = -2\gamma_{\rm inst}$. The evolution is described through the occupation number per state, $N(\boldsymbol{k},\boldsymbol{x})$, the energy density $e_{\rm w}$ being obtained by

$$e_{\rm w} = \int \hbar\omega_k N(k,x)\frac{d^3k}{(2\pi)^3} \qquad \text{(B1)}$$

and the energy flux $\boldsymbol{S}$

$$\boldsymbol{S} = \int \hbar\omega_k\boldsymbol{\upsilon}_{\rm g}(k)N(k,x)\frac{d^3k}{(2\pi)^3} \qquad \text{(B2)}$$

The evolution equation is thus

$$\frac{\partial}{\partial t}N(\boldsymbol{k},\boldsymbol{x})+\boldsymbol{\upsilon}_{\rm g}\cdot\frac{\partial}{\partial\boldsymbol{x}}N(\boldsymbol{k},\boldsymbol{x})=\alpha(\boldsymbol{k})-\beta(\boldsymbol{k})N(\boldsymbol{k},\boldsymbol{x}) \qquad \text{(B3)}$$

we introduce the Lorentz factor $\gamma_{\rm g}$ associated with the group velocity and define the unitary 4-vector $(u_g^\mu) \equiv (\gamma_{\rm g}, \gamma_{\rm g}\boldsymbol{\upsilon}_{\rm g})$. Then the equation can be rewritten as

$$u_g^\mu\nabla_\mu N = \gamma_{\rm g}(\alpha-\beta N)\ . \qquad \text{(B4)}$$

The left hand side of the equation is clearly co-variant. Since N is invariant, the products $\gamma_{\rm g}\alpha$ and $\gamma_{\rm g}\beta$ must be invariant too. In particular we have the important property that the growth rate $\gamma_{\rm inst}$ of an instability is transformed such that the product $\gamma_{\rm g}\gamma_{\rm inst}$ is invariant. This invariant product can be interpreted as the growth rate measured in the wave-frame.

Under a Lorentz transform, the energy density is transformed as follows:

$$\begin{aligned}e'_{\rm w} \quad &= \quad \int\hbar\omega'_kN'(k',x')\frac{d^3k'}{(2\pi)^3}=\int\gamma'_g\hbar\omega'_kN'(k',x')\frac{d^3k'}{\gamma'_g(2\pi)^3}\\ &= \quad \int\gamma_{\rm g}\gamma_0^2\left(1-\frac{\boldsymbol{\upsilon}_{\rm g}\cdot\boldsymbol{\upsilon}_0}{c^2}\right)\left(1-\frac{\boldsymbol{k}\cdot\boldsymbol{\upsilon}_0}{\omega_k}\right)\hbar\omega_kN(k,x)\frac{d^3k}{\gamma_{\rm g}(2\pi)^3}\\ &= \quad \gamma_0^2\int f(k)\hbar\omega_kN(k,x)\frac{d^3k}{(2\pi)^3} \qquad \text{(B5)}\end{aligned}$$

where the factor $f(k) = \left(1-\frac{\boldsymbol{\upsilon}_{\rm g}\cdot\boldsymbol{\upsilon}_0}{c^2}\right)\left(1-\frac{\boldsymbol{k}\cdot\boldsymbol{\upsilon}_0}{\omega_k}\right)$. When the phase velocity is aligned with the group velocity and $\upsilon_\phi\upsilon_g = c^2$, then $f(k) = (1-\boldsymbol{\upsilon}_{\rm g}\cdot\boldsymbol{\upsilon}_0/c^2)^2$ and $\gamma_0^2 f(k) = \gamma_{\rm g}'^2$.

And the energy flux is transformed as follows:

For Weibel modes, that are not eigen-modes of the plasma, it is not clear that such description applies. However this is somewhat simpler, in the case we are treated in this paper, for they have a phase velocity and a group velocity equals to

$$\boldsymbol{\upsilon}_{\rm m}(k_\perp) = \boldsymbol{\upsilon}_{\rm b}\left(1-\xi_{\rm cr}\mu\frac{\gamma_{\rm b}^{-2}+k_\perp^2\delta_e^2}{1+k_\perp^2\delta_e^2}\right)$$

and thus the energy spectrum density $S(k_\perp, x)$ evolves according to

$$\frac{\partial}{\partial t} S + \boldsymbol{v}_{\mathrm{m}} \cdot \nabla S = 2\gamma_{\mathrm{inst}} S \ , \tag{B6}$$

and multiplying both sides of the equation by γ_{m}, the Lorentz factor associated with $\boldsymbol{v}_{\mathrm{m}}$, we obtain a co-variant equation:

$$U_m^{\mu} \nabla_{\mu} S = 2\gamma_{\mathrm{m}}\gamma_{\mathrm{inst}} S \ , \tag{B7}$$

where U_{m}^{μ} is the unitary 4-vector associated with the motion of the magnetic disturbances. Thus, without knowing how S is transformed by Lorentz transformations, we can conclude again that the product $\gamma_{\mathrm{m}}\gamma_{\mathrm{inst}}$ is invariant.